CHAPTER 2

MEASURING THE THERMAL CONDUCTIVITY OF THIN FILMS: 3 OMEGA AND RELATED ELECTROTHERMAL METHODS

Chris Dames

Department of Mechanical Engineering, University of California at Berkeley, 6107 Etcheverry Hall, Berkeley CA 94720-1740, USA; E-mail: cdames@berkeley.edu

This review describes the major electrothermal methods for measuring the thermal conductivity of thin films in both cross-plane and in-plane directions. These methods use microfabricated metal lines for joule heating and resistance thermometry. The 3ω method for cross-plane measurements is described thoroughly, along with a related DC method. For in-plane measurements, several methods are presented for suspended and supported films. Various practical matters are also discussed, including parasitic thermal resistances, background subtraction, and instrumentation issues. The review contains sufficient detail to be accessible to researchers new to the field of thin film thermal conductivity measurements, and also includes information relevant for 3ω measurements of bulk substrates. The review also contains new analytical results for the variable-linewidth 3ω method, the related heat spreader method, and the distinction between isothermal and constant flux heater approximations.

1. INTRODUCTION

1.1 Motivation, Purpose, and Scope

Thin films, superlattices, graphene, and related planar materials are of broad technological interest for applications including transistors, memory, optoelectronic devices, optical coatings, micro-electromechanical systems, photovoltaics, and thermoelectric energy conversion. Thermal performance is a key consideration in many of these applications, motivating experimental efforts to measure the thermal conductivity k of these films.

The thermal conductivity of thin film materials is usually smaller than that of their bulk counterparts, sometimes dramatically so. For example, at room temperature, k of a 20 nm Si film can be a factor of five smaller than its bulk single-crystalline counterpart,[1] and k along the plane of a single layer of encapsulated graphene is at least 10 times smaller than the corresponding value for bulk graphite.[2] Such thermal conductivity reductions generally occur for two basic reasons. First, compared to bulk single crystals, many thin film synthesis technologies result in more impurities, disorder, and grain boundaries, all of which tend to reduce the thermal conductivity. Second, even an atomically perfect thin film is expected to have reduced thermal conductivity due to boundary scattering, phonon leakage, and related interactions. Both basic mechanisms generally affect in-plane (k_x) and cross-plane (k_z) transport differently, so that the thermal conductivity of thin films is usually anisotropic, even for materials whose bulk forms have isotropic k.

ISSN: 1049–0787; ISBN: 978–1–56700–222–6/13/$35.00 + $00.00

NOMENCLATURE

b	heater half-width [m]	β	fin parameter [m^{-1}]
C	volumetric heat capacity [J/m^3K]	λ	thermal wavelength [m]
d	layer thickness [m]	σ	Stefan-Boltzmann constant, 5.67×10^{-8} W/m^2 K^4
D	thermal diffusivity [m^2/s]		
h	heat transfer coefficient for convection and/or radiation [W/m^2K]	θ	temperature difference, $T - T_\infty$ [K]
		τ	thermal diffusion time [s]
I	current [A]	ω	angular frequency [rad/s]
j	$\sqrt{-1}$		
k	thermal conductivity [W/m K]	**Subscripts and Superscripts**	
L	heater length [m]	(unsubscripted)	film
p	probe linewidth [m]	”	area normalized
Q	heat flow [W]	∞	environment
R	thermal resistance [K/W]; with subscript e, electrical resistance [Ω]	0	condition of negligible self-heating (in R_{e0}, the limit $I_1 \to 0$)
T	temperature [K]		
w	half-length of suspended film [m]	1, 2	upper and lower surfaces of film or substrate
V	voltage [V]		
x	in-plane coordinate, normal to the heater length [m]	1ω, 3ω	harmonic number
		c	contact
X	in-phase electrical transfer function [K/W]	char	characteristic
		cond	conduction
y	in-plane coordinate, along the heater length [m]	conv	convection
		e	electrical
Y	out-of-phase electrical transfer function [K/W]	F	film (also unsubscripted)
		H	heater
z	cross-plane coordinate [m]	i	insulation
Z	thermal impedance [K/W]	rad	radiation
		std	standard
Greek Symbols		S	substrate
α	temperature coefficient of resistance [K^{-1}]	x	in plane
		z	cross plane

This review chapter is intended as a detailed introduction to the major electrothermal methods used to measure the thermal conductivity of thin films in both cross-plane and in-plane directions. The scope is strictly limited to techniques where both heating and temperature sensing are electrically based, the most well-known being the “3ω method.”[3] This chapter excludes a large body of techniques that are optically based, such as laser thermoreflectance methods[4–7] and Raman methods.[8–10]

1.2 Audience

This chapter is intended primarily for graduate students and other researchers who are new to this field but desire to perform their own thin film thermal measurements with confidence. Therefore, besides describing the basic principles of the various methods, this chapter details their limits of applicability and the major practical requirements for an accurate measurement.

In addition, readers interested in the traditional 3ω method for *bulk* substrates[11] may find useful information in the discussion of the closely related thin film 3ω method in Sections 2 and 3. Specifically, several of the major measurement issues summarized later in Table 3 are also relevant for measurements of bulk substrates.

Experienced researchers already familiar with thin film thermal measurements may also find some utility in this chapter as a coherent reference to the many measurement issues scattered throughout the primary literature, as exemplified later in Table 3. As a review, this chapter is based largely on previously published results, but specialists may also be interested in a few new results not published elsewhere, as follows:

- Comparison between isothermal and constant–heat flux heater assumptions (Section 3.10)
- Simplified expression for the effective film resistance in the narrow-heater limit [Eq. (18)]
- Sensitivity and limits of applicability for the variable-linewidth 3ω method (Section 6.1)
- Heat spreader method and its connection to variable-linewidth 3ω (Section 6.2 and Fig. 12)
- Issues around the placement of voltage probes in the distributed self-heating method (Fig. 11).

1.3 Related Reviews

Techniques for measuring the thermal conductivity of thin films have been developed intensively since the late 1980s. Among the many articles and books that address the broader field of microscale heat transfer, four reviews in particular have emphasized thin film measurements. Cahill et al.[12] described early uses of the now very well established 3ω method, as well as a related DC method, for cross-plane measurements. Goodson and Flik,[13] Mirmira and Fletcher,[14] and most recently Borca-Tasciuc and Chen[15] each reviewed the contemporaneous state of the art for both in-plane and cross-plane methods, including optical as well as electrothermal methods. Compared to those prior works, the present review gives a refreshed perspective as of 2012, and excludes optical techniques, but goes into greater detail about the electrothermal methods.

1.4 Organization of the Chapter

The first half of this chapter deals with cross-plane measurements, emphasizing the 3ω method. Section 2 introduces the basic concepts, while Section 3 details many of the thermal design and analysis issues. Section 4 then describes various issues related to instrumentation and hardware, with relevance to both cross-plane and in-plane measurements. The chapter ends with in-plane measurements, distinguishing between suspended (Section 5) and supported (Section 6) films. A selection of examples from the literature for these various techniques are summarized in Table 1.

2. CROSS PLANE: BASIC CONCEPTS

2.1 Basic Measurement Concept

Figure 1 shows the basic principle used to measure the cross-plane thermal conductivity of thin films with electrothermal methods. The film of interest (cross-plane thermal conductivity k_z, thickness d) is grown or deposited in intimate contact with a substrate of high thermal conductivity, and a long, narrow strip heater (width $2b$, length L) is then deposited on top of the film. Typical order of magnitude values for selected quantities are given in Table 2. These samples have very fast thermal response times; for example, the thermal diffusion time $\tau \approx L_{\text{char}}^2/D$, where D is the thermal diffusivity, is typically measured in milliseconds for the substrate and microseconds for the film itself.

The sample is placed in a temperature-controlled environment at T_∞. Then electrical current (DC or AC) is passed through the heater, and the resulting joule heating Q causes a small temperature drop $T_{F,1} - T_{F,2}$ through the film. In the case of steady DC heating, all of the heat flows through the substrate and into the environment, whereas a major advantage of AC heating is that the frequency can be chosen to localize the fluctuating temperature field within the film and substrate. The upper film temperature $T_{F,1}$ is frequently approximated as the average heater temperature T_H, which is determined by monitoring changes in the heater's electrical resistance, $R_e(T)$, where the subscript "e" indicates electrical. Strategies for determining the lower film temperature $T_{F,2}$ will be discussed later.

Approximating the heat flow through the film as quasi static and 1D gives

$$R_F = \frac{d}{2k_z bL} \tag{1}$$

where d, b, and L are known and R_F is determined from the experiment using

$$R_F = \frac{T_{F,1} - T_{F,2}}{Q} \tag{2}$$

Of course, many practical issues must be considered for an experiment to be a good approximation of the idealized situation just described. These complications are discussed below in Section 3.

TABLE 1: A selection of references for the major electrothermal techniques used to measure the thermal conductivity of thin films (sources: Refs. 2, 3, 24–28, 30, 33, 43, 70–76, and 78–83). This table is 2 pages wide

References	**Direction**	**Suspended or supported**	**Film**				**Substrate**
			Material	Thickness d [μm]	Extent // to $q^{[a]}$ [μm]	Extent $\perp$ to $q^{[b]}$ [μm]	
3ω method (cross plane)							
3	Cross	Supp.	a-Si:H	0.2 – 1.5	d	∞	Si, MgO
30	Cross	Supp.	a-SiO_2	0.05 – 0.5	d	∞	Si
82	Cross	Supp.	Bi_2Te_3/Sb_2Te_3SL	0.4 – 0.6	d	∞	GaAs
33	Cross	Supp.	Si/SiGe & SiGe/SiGe SLs	3	d	∞	Si
Steady-state cross-plane method							
27	Cross	Supp.	a-SiO_2	0.007 – 0.1	d	∞	Al_2O_3
24	Cross	Supp.	a-SiO_2	1.4	d	∞	Si
13	Cross	Supp.	a-SiO_2	0.29 – 0.36	d	∞	Si
25	Cross	Supp.	a-SiO_2	0.57 – 2.28	d	∞	Si
26	Cross	Supp.	Polyimide	0.5 – 2.1	d	∞	Si
Central line heater method							
70	In	Susp.	Si (doped, poly)	1.5	50 – 100	5 – 10	Si
73	In	Susp.	$Si_3N_4/SiO_2/Si_3N_4$ stack	0.2/0.4/0.2	~ 500	$\sim 10,000$	Si
76	In	Susp.	Diamond	3 – 13	1000	4000	Si
26	In	Susp.	Polyimide	2.2	800	4000	Si
78	In	Susp.	Si	5	500	(?)	Si
72	In	Susp.	Si	3	500	20,000	Si
71	In	Susp.	Si (etched pores)	4 – 7	108	2000	Si

TABLE 1: Continued

References	**Direction**	**Suspended or supported**	**Film**				**Substrate**
			Material	Thickness d [µm]	Extent // to $q^{[a]}$ [µm]	Extent $\perp$ to $q^{[b]}$ [µm]	
Distributed self-heating method							
75	In	Susp.	Al, Ag	0.05 – 0.1	5000	10,000	(?)
74	In	Susp.	Bi	0.02 – 0.4	$>$ 1000(?)	$>$ 1000	Cu
70	In	Susp.	Si (doped, poly)	1.5	50 – 100	5 – 10	Si
79	In	Susp.	Pt	0.028	2.65	0.26	Si
1	In	Susp.	Si	0.02 – 0.1	50 – 250	5 – 20	SOI
Variable-linewidth 3ω method							
43	In (both)	Supp.	Polyimide	1.4 – 2.4	Q varies: $d \times \infty \times \infty$		Si
26	In (both)	Supp.	Polyimide	0.5 – 2.5	Q varies: $d \times \infty \times \infty$		Si
80	In (both)	Supp.	Si/Ge & Ge SLs	1.1 – 1.2	Q varies: $d \times \infty \times \infty$		Si, SOI
Heat spreader method							
81	In	Supp.	Si	0.4 – 1.6	∞	∞	SOI
2	In	Supp.	graphene/graphite	0.0004 – 0.01	15	10	Si

TABLE 1: Continued

References	**Other Layers (e.g., insulation, support, separate heater)**		**Heater**		**Temperature**			**Note**
	Material	Thickness (μm)	Material	Width $2b$ (μm)	How Msr?	Min T [K]	Max T [K]	
3ω method (cross plane)								
3	None		Au	25	TCR	80	400	Differential 3ω (bare substrate)
30	None		Al	28	TCR	293	333	Differential 3ω (vary d), good example of $R_{H-\infty}$ versus d, see Fig. 4(b)
82	Si_3N_4	0.06–0.1	(?)	10–20	TCR	300	300	Differential 3ω (omit SL)
33	Buffer, cap, SiO_2	2, 0.5, 0.1	Au	16–25	TCR	50	320	Differential 3ω (omit SL)
Steady-state cross-plane method								
27	None		Rh (Fe doped)	2	TCR	10	200	Extra T sensor near heater for $T_{F,2}$, see Fig. 4(a)
24	None		Al; poly-Si	100	TCR	120	530	Embedded T sensor for $T_{F,2}$, see Fig. 4(a)
13	None		Al	5	TCR	280	420	Extra T sensor near heater for $T_{F,2}$, see Fig. 4(a). 2D conduction analysis
25	None		Al; poly-Si	100	TCR	263	413	Embedded T sensor for $T_{F,2}$, see Fig. 4(a). 2D conduction analysis
26	Si_xN_y	0.1	Al	100	TCR	260	360	Embedded T sensor for $T_{F,2}$, see Fig. 4(a). Mesa shapes 1D flow

TABLE 1: Continued

References	Other Layers (e.g., insulation, support, separate heater)		Heater		Temperature			Note
	Material	Thickness (μm)	Material	Width $2b$ (μm)	How Msr?	Min T [K]	Max T [K]	
Central line heater method								
70	None		Si (doped)	5	TCR	300	400	
73	None		metal (?)	(?)	TCR	80	400	Emissivity from measuring two samples, D from transient response. 2D conduction analysis
76	None		metal (?)	50	TC	Room T		Microfabricated TCs to measure T. 2D conduction analysis
26	None		Al	4	TCR	260	360	Applies 3ω for in-plane. 2D conduction analysis
78	SiO_2/passive	0.5/1.1	Al; Si (doped)	3 – 4	TCR	100	300	Extra T sensors near heater and substrate help $T_{F,1}$ and $T_{F,2}$, see Fig. 8(b)
72	Polyimide/ LTO/SiO_2	2/0.3/0.34	Al	2	TCR	15	300	Extra T sensors near heater and substrate help $T_{F,1}$ and $T_{F,2}$, see Fig. 8(b)
71	Si_xN_y	0.24	Au	10	TCR	50	300	Extra T sensor near heater and substrate helps $T_{F,2}$, see Fig. 8(b)
Distributed self-heating method								
75	None		(same as film)		ED	300	600	Obtains emissivity from T (x), measure T using electron diffraction
74	Polymer (?)	0.04	(same as film)		TCR	80	400	Get emissivity by measuring second sample, transient response gives D
70	None		(same as film)		TCR	300	400	
79	None		(same as film)		TCR	80	330	
1	Al, CoFe	0.1, 0.075	Al or CoFe	(same as film)	TCR	50	450	Differential (omit Si)

TABLE 1: Continued

References	Other Layers (e.g., insulation, support, separate heater)		Heater		Temperature			Note
	Material	Thickness (μm)	Material	Width $2b$ (μm)	How Msr?	Min T [K]	Max T [K]	
Variable-linewidth 3ω method								
43	Si_xN_y	0.15	Al	1, 5.5, and 200	TCR	Room T (?)		Approximate substrate as isothermal, $k_x/k_z \approx 4-6$
26	Si_xN_y	0.1	Al	4–200	TCR	Room T		Approximate substrate as isothermal (?), $k_x/k_z \approx 6$
80	Si_xN_y	0.1	Metal (?)	2, 30	TCR	80	300	Differential 3ω (omit SL), $k_x/k_z \approx 3-5$
Heat spreader method								
81	SiO_2	0.5	Si (doped)	2	TCR	20	300	1D fin analysis is justified
2	SiO_2	0.03	Au	0.3 – 0.5	TCR	40	300	3D conduction analysis (numerical), validated with Pt film

∞ Very large.
(?) Unclear, unknown, or not given.
d Film thickness.
ED Electron diffraction.
SL Superlattice.
TC Thermocouple.
TCR Temperature coefficient of resistance.
[a] Extent of film parallel to the heat flux direction, corresponding to dimension w of Figs. 8–11. Primarily relevant for in-plane measurements.
[b] Extent of film perpendicular to the heat flux direction, corresponding to dimension L of Figs. 8–11. Primarily relevant for in-plane measurements.

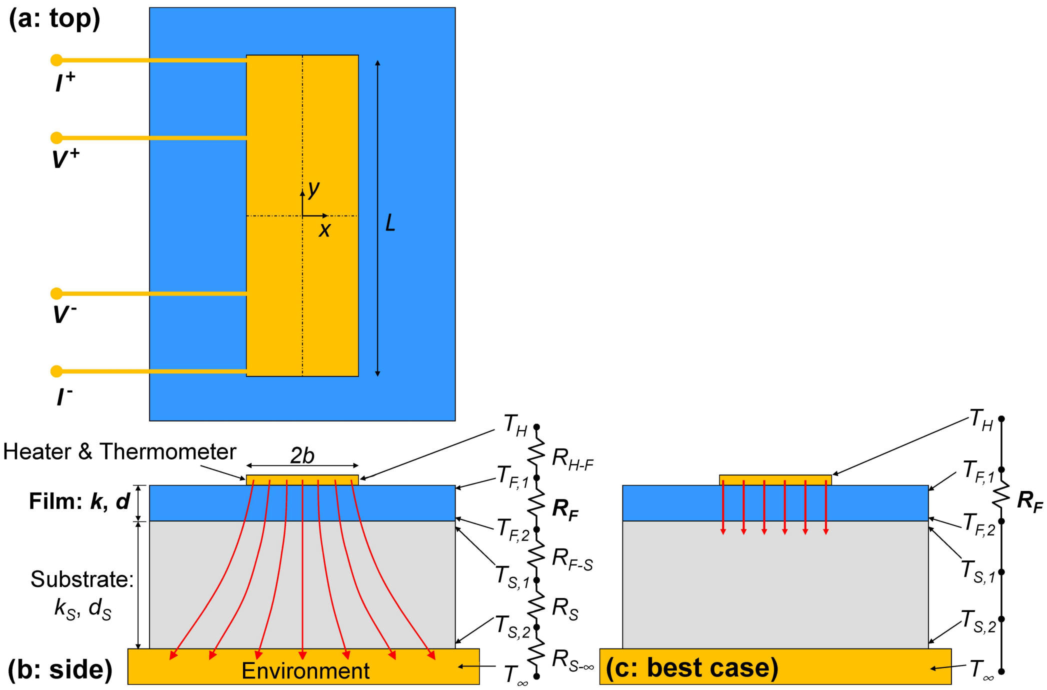

FIG. 1: Measuring the cross-plane thermal conductivity of a thin film using 3ω or steady state methods.

TABLE 2: Typical order of magnitude values in 3ω experiments to measure the cross-plane thermal conductivity of a thin film. Representative heater dimensions are half-width $b = 20$ μm and length $L = 2000$ μm. The thermal wavelength is given at a typical heater frequency of 5000 rad/s (electrical current of around 400 Hz)

		Thickness, d	**Thermal conductivity,** k	**Heat capacity,** C	**Thermal wavelength at** $\mathbf{w}_H$ **= 5000 rad/s,** $\lambda = \sqrt{D/\omega_H}$
	Typical materials	**[μm]**	**[W/m K]**	**[J/m^3 K]**	**[μm]**
Heater	Au, Pt, Al	0.2	100	2×10^6	100
Thin film	a-SiO_2, polymer, superlattice	0.5	1		10
Substrate	Si, Al, MgO, GaAs	500	150		120

2.2 AC Response: 3ω Methods and Beyond

In the case of steady DC heating, it is straightforward to determine T_H from measurements of the heater's current and voltage and its previously calibrated $R_e(T)$ curve. However, when the heater is driven with a sinusoidal current, some care is needed to correctly analyze all of the resulting voltage signals, requiring attention to the coupling between electrical and thermal domains and the various harmonics. The basic idea is as follows (Fig. 2). The electrical current at angular frequency ω causes joule heating at DC and 2ω. Because the response in the thermal domain is linear, this 2ω heating causes temperature fluctuations also at 2ω, with an amplitude and phase that depends on the thermal properties of the system. This perturbs the heater's electrical resistance at 2ω, which when multiplied by the driving current at ω finally causes a small voltage signal across the heater at a frequency 3ω. Thus, this class of measurements is aptly known as "3 omega" methods, and was first applied to measure the thermal conductivity of films and substrates by Cahill and coworkers.[3,11,12,16]

We now show how this 3ω voltage depends on the sample's thermal properties. To keep the analysis general, the sample's thermal response is initially described by a generic thermal transfer function in the frequency domain, Z, which relates the average temperature rise of the heater to the heat input, Q. The general solution of the combined electrothermal problem for all harmonics and arbitrary Z was derived in Ref. 17. In terms of Fig. 2, if the heater is driven at

$$Q(t) = Q_0 \sin(\omega_H t) \tag{3}$$

its temperature response is

$$T_H(t) - T_\infty = Q_0 \left[\mathrm{Re}(Z)\sin(\omega_H t) + \mathrm{Im}(Z)\cos(\omega_H t)\right] \tag{4}$$

To link this thermal response with the electrical domain, we focus on the simplest case where the heater is driven with a sinusoidal current,

$$I = I_{1\omega}\sin(\omega t) \tag{5}$$

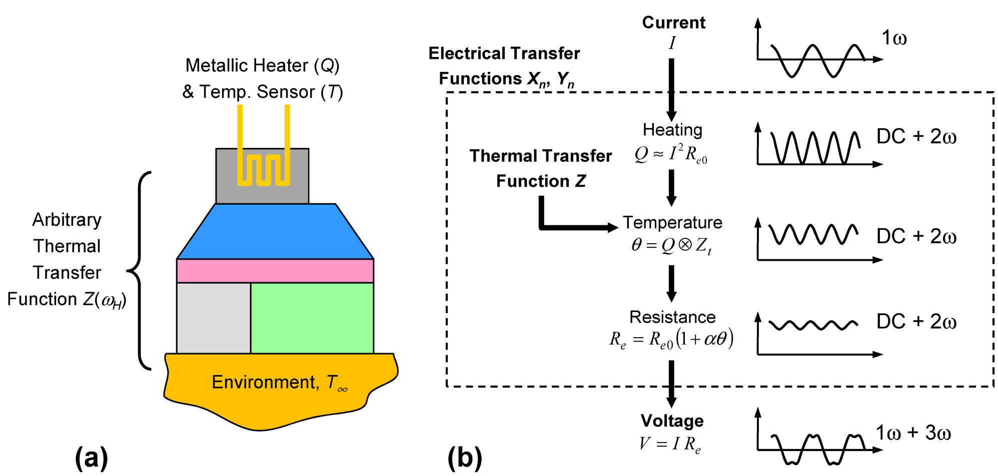

FIG. 2: (a) A generic system whose thermal transfer function $Z(\omega_H)$ can be measured using an electrothermal technique such as the 3ω method.[17] The different colored blocks represent arbitrary materials and geometries. (b) Relationships between sinusoidal current and voltages and the thermal transfer function, used to understand the generic 3ω method. (Here $\otimes$ denotes convolution and Z_t is the inverse Fourier transform of Z.)

where the current is defined in terms of sine rather than cosine to be consistent with certain commercial lock-in amplifiers. In this case the rms voltages at the various harmonics $n\omega$ can be expressed as[17]

$$\frac{V_{n\omega,\text{rms}}}{2\alpha R_{e0}^2 I_{1\omega,\text{rms}}^3} = X_{n\omega}(\omega) + jY_{n\omega}(\omega) \tag{6}$$

where $R_{e0}(T) = \lim\left[V_{1\omega}/I_{1\omega}\right]_{I\to 0}$ is the zero-current electrical resistance at the temperature being measured, $\alpha(T) = (1/R_{e0})/(dR_{e0}/dT)$ is the temperature coefficient of resistance, $I_{1\omega,\text{rms}} = I_{1\omega}/\sqrt{2}$, $j = \sqrt{-1}$, and $X_{n\omega}$ and $Y_{n\omega}$ are the in-phase and out-of-phase electrical transfer functions.

Expressions for all eight transfer functions ($X_{n\omega}$, $Y_{n\omega}$, n = 0...3) are given in Table 1 of Ref. 17. Here we give only those for the third harmonic voltages, which are the most useful in practice because they are directly proportional to the real and imaginary parts of the thermal transfer function at a single frequency,

$$X_3(\omega) = -\frac{1}{4}\text{Re}\left[Z(2\omega)\right] \tag{7a}$$

$$Y_3(\omega) = -\frac{1}{4}\text{Im}\left[Z(2\omega)\right], \tag{7b}$$

so that

$$V_{3\omega,\text{rms,in-phase}} = -\frac{1}{2}\alpha R_{e0}^2 I_{1\omega,\text{rms}}^3 \text{Re}\left[Z(2\omega)\right] \tag{8a}$$

$$V_{3\omega,\text{rms,out-of-phase}} = -\frac{1}{2}\alpha R_{e0}^2 I_{1\omega,\text{rms}}^3 \text{Im}\left[Z(2\omega)\right] \tag{8b}$$

Thus, for a driving current at ω, the voltage at 3ω is directly proportional to the thermal transfer function at 2ω. (For example, a current at 500 rad/s causes a voltage at 1500 rad/s related to the system's thermal response at 1000 rad/s.) This means that the entire thermal transfer function is readily obtained using a frequency sweep.

It is sometimes desirable to have explicit expressions for the temperature fluctuations,

$$\theta(t) = \theta_{\text{DC}} + \theta_{2\omega,\sin}\sin(2\omega t) + \theta_{2\omega,\cos}\cos(2\omega t) \tag{9}$$

where $\theta \equiv T - T_\infty$. For the 2ω temperature fluctuations, it is readily shown that

$$\theta_{2\omega,\cos,\text{rms}} = \frac{\sqrt{2}\,V_{3\omega,\text{rms,in-phase}}}{\alpha R_{e0}\,I_{1\omega,\text{rms}}} \tag{10a}$$

$$\theta_{2\omega,\sin,\text{rms}} = \frac{-\sqrt{2}\,V_{3\omega,\text{rms,out-of-phase}}}{\alpha R_{e0}\,I_{1\omega,\text{rms}}} \tag{10b}$$

This is equivalent to the expression given by Cahill,[11,18] whose quantity ΔT is equivalent to the amplitude $\theta_{2\omega}$ here. Similarly, it can also be shown that

$$\theta_{\text{DC}} - \frac{1}{\sqrt{2}}\theta_{2\omega,\cos,\text{rms}} = \frac{V_{1\omega,\text{in-phase,rms}} - I_{1\omega,\text{rms}}R_{e0}}{\alpha I_{1\omega,\text{rms}}R_{e0}} \tag{11a}$$

$$\frac{1}{\sqrt{2}}\theta_{2\omega,\text{sin,rms}} = \frac{V_{1\omega,\text{out-of-phase,rms}}}{\alpha I_{1\omega,\text{rms}} R_{e0}} \tag{11b}$$

As we shall briefly mention in Section 3.2 the primary utility of Eqs. (11) is in estimating the DC temperature rise to confirm that it may be neglected.

2.3 Advantages of AC methods

The general sample configuration shown in Fig. 1 applies to both AC and DC measurement methods. As suggested by Table 1, DC methods were used primarily in the 1990s while most more recent works have emphasized the 3ω method, which as an AC approach offers several important advantages.

2.3.1 Insensitive to Boundary Condition between Substrate and Environment ($R_{S-\infty}$)

As shown in Fig. 3, the heating frequency is generally chosen such that the thermal wavelength in the substrate,[11]

$$\lambda_S = \sqrt{\frac{D_S}{\omega_H}} \tag{12}$$

where D_S is the thermal diffusivity of the substrate, is several times smaller than the substrate thickness d_S. Thus, because the oscillating portion of the thermal signal is localized well within the substrate, the AC thermal response is insensitive to the boundary condition between the substrate and environment, indicated as $R_{S-\infty}$ in Fig. 1. This is beneficial because such contact resistances are generally poorly controlled and may not be negligible, so removing them simplifies the analysis and interpretation. This also helps improve sensitivity by increasing the fraction of the total temperature drop ($T - T_\infty$) that occurs across the film. However, it should also be remembered that the DC thermal response always experiences the full resistance path from heater to substrate, increasing the average temperature of the film (Section 3.2).

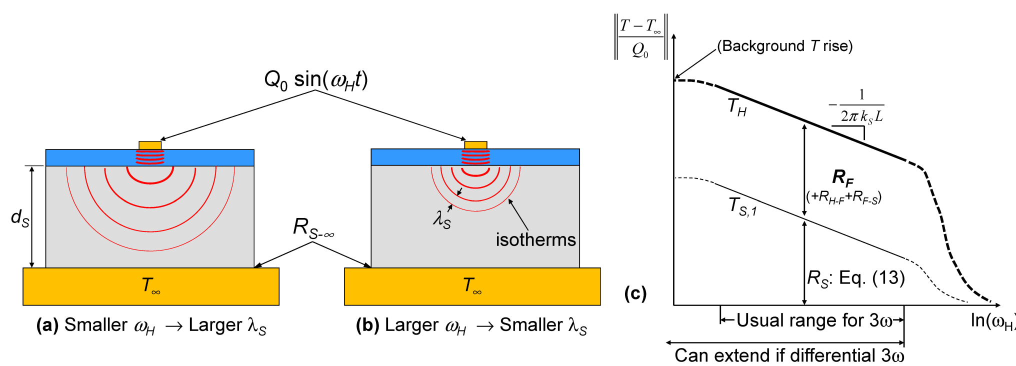

FIG. 3: The 3ω method to measure the cross-plane thermal conductivity of a thin film. (a,b) Schematics of the temperature field at two different frequencies. (c) Frequency dependence of the temperature rise.

2.3.2 Quantifying and Reducing the Substrate Contribution (R_S)

A related benefit is that the effective value of R_S can also be reduced by increasing ω_H. For the strip-heater configuration at moderately low frequencies ($b \ll \lambda_S \ll d_S$),

$$Z_S = \frac{1}{\pi L k_S}\left[\ln\left(\frac{\lambda_S}{b}\right) + \eta - j\frac{\pi}{4}\right] \tag{13}$$

where $\eta \approx 0.923$ [the analytical result[19] for η is exactly 3/2 minus the Euler constant, although in early work a value $\eta = 1.05$ was reported to be in better agreement with experiments].[20] Note that the first term in Eq. (13) is exactly the radial conduction resistance of a cylindrical half shell of inner radius b and outer radius λ_S. Thus, by increasing the heater frequency, the effective R_S is somewhat reduced, further improving the sensitivity of $T_H - T_\infty$ to R_F, as well as the thermal response time. Although beyond the scope of this article, we also note in passing that measuring the slope of $V_{3\omega,\mathrm{rms}}$ with respect to $\ln(\omega)$ is the basis of an important method for measuring k_S, the original "3ω method."[11]

2.3.3 Less Sensitive to Radiation and Convection Losses

Equation (13) shows that the thermally active volume of the sample extends only a distance of order λ_S into the substrate. This is equivalent to using a substrate shaped as a half cylinder of length L and radius $\sim \lambda_S$, which as pointed out by Cahill[11] is favorable for minimizing the impact of heat losses. We give the basic argument here. Heat is lost from the top surface to the surroundings by radiation and, if the sample is not in high vacuum, by convection. These effects are considered jointly using a combined heat transfer coefficient h for convection plus radiation, $h = h_{\mathrm{conv}} + h_{\mathrm{rad}}$, where

$$h_{\mathrm{rad}} = 4\varepsilon\sigma T_{\mathrm{avg}}^3 \tag{14}$$

T_{avg} is the average temperature of the sample and surroundings, ε is the emissivity of the sample surface, and σ is the Stefan-Boltzmann radiation constant. We now consider two limiting cases.

First, the best case is when R_F dominates the total thermal resistance. In this case, there is no particular sensitivity advantage of AC versus DC methods with regard to radiation and convection, and both are very robust against such losses. The conduction heat flow is $Q_{\mathrm{cond}} = 2kbL(T_H - T_\infty)/d$, while the losses are $Q_{\mathrm{rad+conv}} = 2hbL(T_H - T_\infty)$, so that the loss ratio is simply the film Biot number, $Q_{\mathrm{rad+conv}}/Q_{\mathrm{cond}} \approx hd/k$. For typical films of $k \approx 1$ W/m K and $d \approx 1$ μm, the losses are <1% as long as $h <$ 10,000 W/m^{2}K, which is very easily satisfied. For example, typical values are $h_{\mathrm{rad}} <$ 230 W/m^{2}K for radiation at $T <$ 1000 K and $h_{\mathrm{conv}} \approx$ 2–25 W/m^2 K for natural convection in air.[21] (Note that these values of h_{conv} are appropriate for macroscopic samples. Values for the microscopic heater strips as used in 3ω experiments are not readily apparent in the literature but will be subject to two competing effects. The narrower heater width tends to increase h_{conv}, while the surrounding unheated substrate tends to impede air flow and reduce h_{conv}.) Another limit is when R_S dominates the total thermal resistance, and it is this case where the AC method does offer a potential advantage[11] compared to the DC approach. In this limit $Q_{\mathrm{rad+conv}}$ scales as $h\lambda_S L(T_H - T_\infty)$, while from Eq. (13), Q_{cond} scales as $\pi k_S L(T_H - T_\infty)$, ignoring the weak logarithmic function in square brackets of Eq. (13). Thus, the relative impact of heat losses is

$$\frac{Q_{\text{rad+conv}}}{Q_{\text{cond}}} \approx \frac{h\lambda_S}{2k_S} \tag{15}$$

where the correct prefactor $1/2$ has been obtained from Ref. 11. For a typical experiment with $\lambda_S \approx 100$ μm and $k_S \approx 100$ W/m K, the losses are <1% if $h < 20{,}000$ W/m^{2}K, which as noted above is very easily satisfied. In contrast, DC measurements on larger samples with characteristic lengths at the centimeter scale would reduce the threshold h to the low 100s of W/m K.

2.3.4 Insensitive to DC Voltage Artifacts from Thermoelectric Effects and Low-Frequency Drifts

For experiments requiring the utmost accuracy, AC methods are also beneficial because by moving the measurement away from DC, they can minimize the impacts of $1/f$ noise and other low-frequency drifts. For example, one possible source of such drifts is the use of several metals with dissimilar Seebeck coefficients. A typical cryostat experiment might use gold for the heater line and wire bonding, constantan for connections inside the cryostat, and copper wires outside. The important junctions are those along the path of the two voltage probes used in four-probe resistance thermometry. For example, if the V^+ and V^- junctions at a feedthrough connector have their temperatures evolve differently over the course of an experiment, the resulting thermoelectric voltage drifts cause artifacts that could be misinterpreted as changes in the sample resistance. Such thermoelectric artifacts are absent in AC measurements, as well as in DC measurements that average voltages obtained from forward and reverse current polarities. It is also good practice to ensure that any junctions between dissimilar metals are located in regions of the cryostat that are locally isothermal at any given time.

3. CROSS PLANE: THERMAL DESIGN AND ANALYSIS

In this section, we describe various thermal issues that are important for the cross-plane measurement method shown in Figs. 1 and 3, with major emphasis on the 3ω method first presented by Cahill et al.[3] After presenting the important differential 3ω method and a comment about the background temperature rise, this section is organized around Table 3, which summarizes the major thermal design issues. As a concrete example, Table 4 summarizes numerical results for these design issues for a specific case study, based on the representative parameters from Table 2.

3.1 Determining the T Drop Across the Film: The Differential 3ω Method

Referring to Fig. 1, the most obvious challenge in these measurements is to determine the temperature drop across the film. Here we briefly describe strategies for determining $T_{F,1}$ and $T_{F,2}$, and then the very important differential 3ω method.

TABLE 3: Summary of thermal design rules for 3ω measurements of the cross-plane thermal conductivity of films. Note the distinction between the thermal wavelengths in the film (λ) and the substrate (λ_S), which typically differ by an order of magnitude (Table 2). Approximations iv–vi and ix are also relevant for 3ω measurements of k_S of bulk substrates[11]

	Desired approximation	Criteria	References	Notes
i	Substrate is isothermal ($k_S \to \infty$)	Error $\approx (k/k_S)^2$	42	• Usually safely neglected; else use known correction factor
ii	Film heat flow is 1D (neglect edge effects)	$(b/d)(k_z/k_x)^{1/2} > 5.5$ for 5% error $(b/d)(k_z/k_x)^{1/2} > 30$ for 1% error	42	• Error cannot be removed by differential 3ω • If heater is not wide enough but substrate approx. isothermal, use Eqs. (16), (17), or (18) • Or, pattern micro-mesa[24,26,32]
iii	Film heat flow is quasi-static ($C \to 0$)	$\lambda/d > 2.5$ for 5% error $\lambda/d > 5.7$ for 1% error	44	• Error cannot be removed by differential 3ω • Possible concern for films of very low k; use lower w_H
iv	Substrate is semi-infinite ($d_S \to \infty$)	$d_S/\lambda_S > 5$ for 1% error	42	• Smaller d_S/λ_S is acceptable for differential 3ω • Exact solution is known for any d_S/λ_S
		$d_S/\lambda_S > 2$ appears acceptable	45	
v	Substrate sees heater as line source ($b \to 0$)	$\lambda_S/b > 2.1$ for 5% error $\lambda_S/b > 5$ for 1% error	42	• Smaller λ_S/b is acceptable for differential 3ω • Exact solution is known for any λ_S/b
		$\lambda_S/b > 1.6$ for 5% error	47	
vi	Heater is infinitely long ($L \to \infty$)	$L/\lambda_S > 4.7$ for 1% error in 4-pad config. $L/\lambda_S > 15$ for 1% error in 2-pad config.	45	• 4 pad is recommended • Smaller L/λ_S is acceptable for differential 3ω
vii	Heater is massless ($C_H d_H \to 0$)	Errors approximately $(C_H/C)(d_H d/\lambda^2)$	42, 44	• Errors usually small because often $\lambda > d \gg d_H$
viii	Heater is uniform heat source	Safe to neglect lateral heat redistribution within heater if $(d_H d/b^2)(k_H/k) \ll 1$	(This work)	• Usually neglected. Errors of <3% for $(b/d)(k_z/k_x)^{1/2} > 4.8$ • Error cannot be removed by differential 3ω
ix	Convection and radiation negligible ($h \to 0$)	$Q_{\text{rad+conv}}/Q_{\text{cond}} \approx \max(hd/k, h\lambda_S/2k_{\text{Sub}})$	11	• Usually well satisfied • See also Section 2.3, Eq. (15)

TABLE 4: Numerical case study of the thermal design rules of Table 3, evaluated for the representative example of Table 2. Shading indicates conditions where the errors are expected to exceed 3%. For issues iv, v, and vi, the errors can be subtracted out using the differential 3ω method

				Value at driving current of $\omega/2\pi$ =			
	Desired approximation	**Parameter**	**Target (for 1% error)**	**10 Hz**	**100 Hz**	**1000 Hz**	**10,000 Hz**
i	Substrate is isothermal	$(k/k_S)^2$	< 0.01	$\sim 10^{-5}$			
ii	Film heat flow is 1D	$(b/d)(k_z/k_x)^{1/2}$	> 30	40			
iii	Film heat flow is quasi static	λ/d	> 5.7	126	40	13	4.0
iv	Substrate is semi-infinite	d_S/λ_S	> 2	0.65	2.1	6.5	20
v	Substrate sees heater as line	λ_S/b	> 5	39	12	3.9	1.2
vi	Heater is infinitely long	L/λ_S	> 4.7	2.6	8.2	26	82
vii	Heater is massless	$(C_H/C)(d_H d/\lambda^2)$	< 0.01	3×10^{-5}	3×10^{-4}	3×10^{-3}	3×10^{-2}
viii	Heater is uniform heat source	$(d_H d/b^2)(k_H/k)$	$\ll 1$	0.025			
ix	Convection and radiation negligible (take h = 200 W/m^{2}K)	max[(hd/k),$(h\lambda_S/2k_{\mathrm{sub}})$]	< 0.01	5×10^{-4}	2×10^{-4}	1×10^{-4}	1×10^{-4}

The upper film temperature $T_{F,1}$ is essentially always taken to be equal to the heater temperature T_H, which requires neglecting R_{H-F} compared to R_F. This is usually a good assumption for metallic heaters deposited directly on dielectric films, for which the thermal contact resistances R_c'' are typically 10^{-8}–10^{-7} m^{2}K/W.[22,23]

Determining the lower film temperature $T_{F,2}$ is a greater challenge. As noted above, one of the major advantages of AC experiments is that the heating frequencies can be chosen to localize the oscillating temperature field within the film and substrate, eliminating $R_{S-\infty}$ and making R_S amenable to exact analytical calculation. Thus, probably the most common method to determine $T_{F,2}$ is to calculate it from the experimental heat flux and R_S from equations such as Eq. (13). This requires knowledge of k_S, which itself may be measured directly from the "slope method" mentioned below Eq. (13), or estimated from handbook values. This calculation is far more forgiving for substrates with large k_S as compared to k of the film (see also Section 3.3).

A less common method to determine $T_{F,2}$ is to measure it using a nearby T sensor, as shown in Fig. 4(a). Embedding a T sensor between film and substrate,[24–26] as in Fig. 4(a) (left), complicates the microfabrication but is the closest realization of a direct measurement of $T_{F,2}$. Alternatively, no additional microfabrication steps should be necessary to create a sensor on top of the film nearby the heater, as shown in Fig. 4(a) (right). However, care is required to ensure that the T measured by this additional sensor faithfully represents the actual $T_{F,2}$.[13,27,28] Specifically, to avoid erroneous detection of the edge effects of heat spreading in the film [see Fig. 5(b) below], a gap should be allowed between the sensor and the heater. Assuming an isothermal substrate, the numerical results show that the gap width should be at least 1.6 times the film thickness d to keep the errors below 5%, or 2.6d to keep the errors below 1%. If the film is anisotropic, the same criteria apply to $d(k_x/k_y)^{1/2}$.

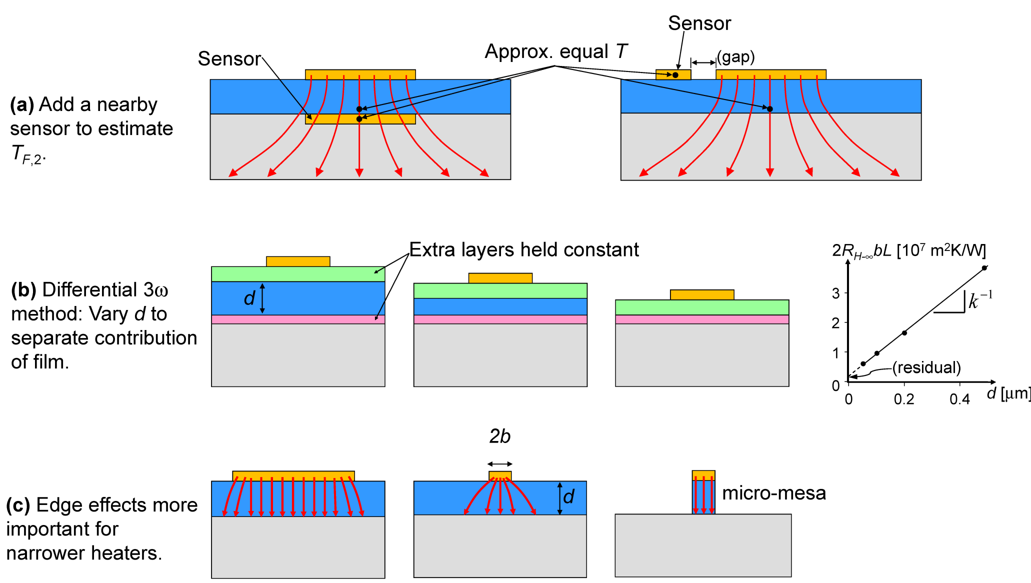

FIG. 4: Further considerations for the 3ω method. The plot in (b) represents measurements of amorphous SiO_2 films from Ref. 30.

Such measurements of $T_{F,2}$ have previously all been for DC-based measurements,[13,24–28] perhaps because DC methods are more prone to errors in determining R_S and $R_{S-\infty}$ than the 3ω method.

3.1.1 The Differential 3ω Method

For many samples, a "differential 3ω method" is the best way to account for the difficulties in determining $T_{F,1}$ and $T_{F,2}$.[29–33] This is particularly important for samples such as superlattices, which commonly require additional buffer and/or cap layers for sample growth, adding undesirable series resistances to R_{H-F} and R_{F-S}. As shown in Fig. 4(b), the key concept is to prepare a set of samples identical in every way except for varying the film thickness d. This ideally includes a control sample without any film (d = 0). In this way, the control sample can be used to subtract out the common background contribution of $(R_{H-F} + R_{F-S} + R_S + R_{S-\infty})$ from all measurements, leaving only R_F as a function of d. (Note that this requires a subtle assumption, because once the film is absent the nature of the contact resistances changes. It is usually assumed that $R_{H-F} + R_{F-S}$ remains constant even in the control case of no film, although as is apparent from Fig. 4(b), there are one fewer interfaces once the film is absent, and the mating materials are also different. This assumption should be acceptable for all but the thinnest, most conductive films.) Furthermore, in films where the important mean free paths of the energy carriers[34–36] are small compared to d, the thermal transport in the film can be expected to be fully diffusive.[37,38] In this case, a plot of $R_{H-\infty}$ against d should be a straight line with slope $1/2kbL$ and intercept representing the background terms $(R_{H-F} + R_{F-S} + R_S + R_{S-\infty})$. An example of data of this sort is given in Fig. 4(b) for SiO_2 films.[30] This linear relation only holds if the microstructure and thus k of the deposited film is independent of d.

As detailed in the remainder of this section, this thermal background subtraction inherent in the differential 3ω method can eliminate many (though not all) of the major nonidealities in practical experiments. Of course, for best sensitivity, the experiment should still be designed for R_F to make up as large a fraction of the total $R_{H-\infty}$ as possible.

3.2 Background Temperature Rise at Steady State

The heater power in a 3ω experiment is typically chosen such that the temperature oscillation $\theta_{2\omega}$ is a small fraction of the absolute environment temperature, and then T_∞ is taken as representative of the property being measured. Although this is generally a good approximation, it should be remembered that the oscillating 2ω heating power of interest is always superposed on a background DC power, of magnitude equal to the amplitude of the 2ω power oscillation [Fig. 2(b)]. This steady heating always experiences the full resistance chain from heater to environment, $R_{H-\infty}$, even though the fluctuating temperature field is usually localized to be insensitive to $R_{S-\infty}$ and much of R_S.

Thus, this background heating effect always causes the average sample temperature to be higher than T_∞.[39–41] In the best case R_F dominates the total $R_{H-\infty}$, and a fluctuating temperature amplitude of, for example, $\theta_{2\omega}$ = 4 K, will be accompanied by a DC temperature rise also of θ_{DC} = 4 K. In this case, if a film's k was measured in an environment at T_∞ = 300 K, then $T_{F,2}$ also is 300 K, while $T_{F,1}$ oscillates sinusoidally between 300 and 308 K. Thus, the measured k corresponds to an average film T of 302 K (the spatial average of 304 and 300 K), a minor correction that is commonly ignored.

However, if the sample is poorly heat sunk to the surroundings, it is not implausible that R_F could make up only one-tenth of $R_{H-\infty}$. Now the same temperature fluctuation amplitude of $\theta_{2\omega}$ = 4 K will be accompanied by a DC temperature rise of θ_{DC} = 40 K. In this case, if T_∞ = 300 K the time-averaged values of $T_{F,1}$ and $T_{F,2}$ are 340 and 336 K, respectively, and thus the average film temperature is really 338 K, rather than 300 K, which might otherwise be assumed. This problem is usually not an issue if the substrate has high thermal conductivity and care was taken to mount the sample using appropriate grease, paste, soft foil, and/or clamping pressure. However, it is more likely to be a concern in cryogenic environments[39] because the thermal conductivity of most substrates and supporting materials dies off at low T. Fortunately, it is straightforward to check for, and if necessary correct for, this background DC heating issue[39,40] by monitoring the 1ω voltages and using Eq. (11a).

3.3 Substrate Contrast [Table 3 (i)]

The 3ω method is most sensitive to the film's thermal conductivity when it is much smaller than that of the substrate. This effect was considered analytically by Borca-Tasciuc et al.,[42] who showed that the errors are approximately $(k/k_S)^2$. These errors are usually safely below 1%, because in typical experiments the substrate thermal conductivity is $\sim$100 W/m K or larger (e.g., undoped Si), while the film's k is well below 10 W/m K. However, caution is required for lower k_S substrates (e.g., glass or quartz) or more thermally conductive films.

3.4 Edge Effects and the Heater Width for 1D Cross-Plane Flow [Table 3 (ii)]

The ideal configuration depicted in Fig. 1 presumes 1D heat conduction across the film. However, even in the best case of an isothermal substrate ($k_S \to \infty$) it is obvious that there will be edge effects at $x = \pm b$. Representative calculations for a uniform heat source are shown in Fig. 5 for three different dimensionless heater widths, $(\mathrm{b}/d)(k_z/k_x)^{1/2}$. [This nondimensionalization allows for an anisotropic thermal conductivity tensor in the film, which we shall return to later, and arises naturally from nondimensionalizing an anisotropic Laplace equation $k_x(\partial^2 T/\partial x^2) + k_z(\partial^2 T/\partial z^2) = 0$.]

From Fig. 5, it is clear that the edge effects increase the effective cross-sectional area for heat conduction, which must reduce R_F compared to the expression of Eq. (1). This effect has been considered analytically for a uniform heat source by Borca-Tasciuc et al.,[42] who in the best case of an isothermal substrate ($k_S^2 \gg k_x k_z$) obtained

$$\frac{R_F}{d/2k_z bL} = \frac{2}{\pi}\left(\frac{b}{d}\right)\left(\frac{k_z}{k_x}\right)^{1/2}\int_0^\infty u^{-3}\sin^2(u)\tanh\left[u\left(\frac{d}{b}\right)\left(\frac{k_x}{k_z}\right)^{1/2}\right]du \tag{16}$$

This result gives the actual film resistance normalized to the value for purely cross-plane conduction, as a function of the dimensionless heater width. This function is plotted in

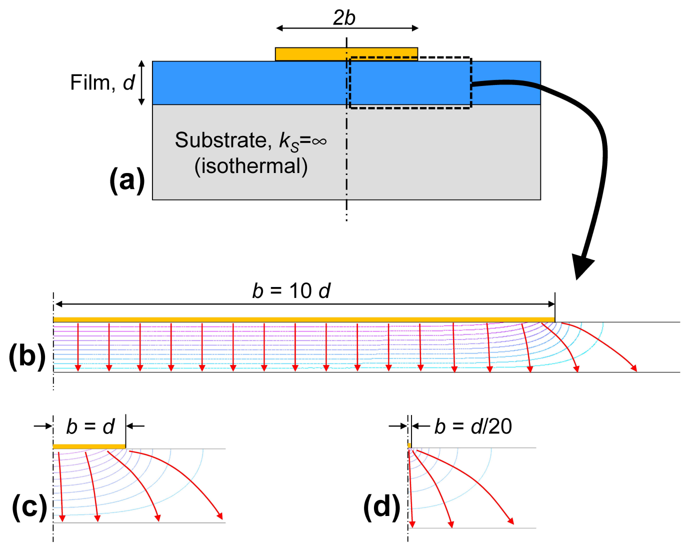

FIG. 5: Edge effects and lateral heat spreading for a heater with uniform heat flux and finite width. The isotherms in (b–d) are exact results from a numerical calculation, while the heat flux lines were sketched by hand. For accurate cross-plane 3ω measurements of k_z, these edge effects should be minimized, while they are exploited to advantage in the variable-linewidth 3ω method to measure k_x.

Fig. 6(a) and is within 5% of unity for $(b/d)(k_z/k_x)^{1/2} > 5.5$, and within 1% of unity for $(b/d)(k_z/k_x)^{1/2} > 30$. In circumstances where further control of the lateral spreading errors is required, they can be virtually eliminated by shaping the film as a micromesa with the heater integrated on top [Fig. 4(c), right panel].[24,26,32] A convenient and physically appealing approximation to Eq. (16) is to retain the 1D form of Eq. (1) but simply increase the effective heater width to account for the increased heat transfer, using[42]

$$b_{\text{eff}} = b + 0.38d\left(\frac{k_x}{k_z}\right)^{1/2} \tag{17}$$

This approximation is shown by the dashed line in Fig. 6(a). It is helpful for all but the narrowest heaters, being within 3% of the exact result of Eq. (16) for all $(b/d)(k_z/k_x)^{1/2} > 0.1$.

In the opposite limit of a narrow heater, we find here that the integral of Eq. (16) has the asymptotic approximation $(b/d)(k_z/k_x)^{1/2}[0.66745 + (2/\pi)\ln(d/b)(k_x/k_z)^{1/2}]$, so that

$$R_F \approx \left(\frac{1}{2L}\right)\left(\frac{1}{k_z k_x}\right)^{1/2}\left[0.66745 + \frac{2}{\pi}\ln\left(\left(\frac{d}{b}\right)\left(\frac{k_x}{k_z}\right)^{1/2}\right)\right] \tag{18}$$

where the logarithmic term is reminiscent of the radial conduction resistance for a cylindrical shell, consistent with the isotherms of Fig. 5(d). Equation (18) is within 1% of the exact result of Eq. (16) for all $(b/d)(k_z/k_x)^{1/2} < 0.4$.

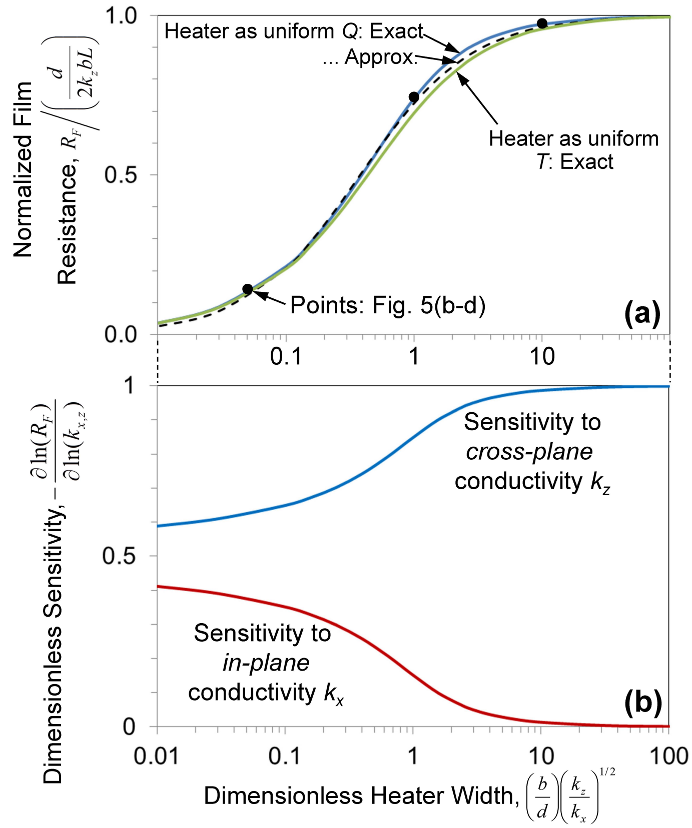

FIG. 6: Edge effects and lateral heat spreading for finite heater width, which can be exploited to measure k_x using the variable-linewidth 3ω method. All calculations assume a perfectly isothermal substrate. (a) The actual film resistance R_F becomes smaller than the ideal 1D resistance as the heater becomes narrower. (b) For wide heaters, R_F is sensitive only to the cross-plane conductivity, while for narrow heaters, R_F is sensitive to the conductivities in both directions. The calculation in (b) is based on the uniform-Q approximation, and the uniform-T approximation differs only slightly.

Equations (16)–(18), as with almost all of this article and the published literature, approximate the real heater line as a uniform heat source, thereby neglecting any heat redistribution within the heater line. The opposite limiting approximation is to treat the heater as isothermal (see also Section 3.10), in which case an analytical result for R_F has been obtained by Ju et al.[43] in terms of elliptical integrals. This function is also shown in Fig. 6(a). The solution yields 5% and 1% error threshold values for $(b/d)(k_z/k_x)^{1/2}$ of 8.4 and 44, respectively, when compared to the uniform 1D assumption of Eq. (1). These thresholds are slightly more restrictive than those given above for a constant-Q heater. For an isothermal heater, there is also a simple effective-linewidth expression like Eq. (17), but with 0.44 in place of 0.38,[3] which is within 3% of the exact result[43] as long as $(b/d)(k_z/k_x)^{1/2} >$ 0.23.

3.5 Maximum Frequency for Quasi-Static Heat Conduction through Film [Table 3 (iii)]

The standard analysis neglects the heat capacity of the film, which is a good approximation for $\lambda \gg d$. A more detailed analysis by Ju and Goodson[44] showed that the thermal impedance of the film includes a multiplicative factor $\lambda/d \tanh(d/\lambda)$. This factor is within 1% of unity for $\lambda/d > 5.7$, and within 5% of unity for $\lambda/d > 2.5$. On the other hand, if the frequency range extends high enough that $\lambda/d < 1$ can be achieved, the measurements can be used to determine the film's thermal diffusivity as well.[44]

3.6 Substrate Thickness to be Semi-Infinite [Table 3 (iv)]

As noted above it is helpful, though not essential, if the substrate can be approximated as semi-infinite, which requires $d_S \gg \lambda_S$. This issue was considered quantitatively by Borca-Tasciuc et al.,[42] who recommended $d_S/\lambda_S > 5$ to keep errors below 1%. The numerical results of Jacquot et al.[45] suggest that even for $d_S/\lambda_S \approx 2$ the semi-infinite solutions appear to be a good approximation. When the wavelength is longer, the boundary condition $R_{S-\infty}$between substrate and environment begins to matter, and solutions are known for isothermal, adiabatic, and arbitrary contact resistance boundaries.[30,42]

3.7 Substrate Sees Heater as a Line Source [Table 3 (v)]

It is also convenient if b is small enough compared to λ_S for the line source result of Eq. (13) to be a good approximation for the substrate's temperature rise. This is not essential because various full analytical solutions are known for arbitrary linewidth.[30,40,42,46,47] Comparisons of Eq. (13) with the exact solutions from Refs. 42 and 47 show that λ_S/b should be larger than around 5 to keep the errors at $<$1%.

3.8 Heater Length to Neglect End Effects [Table 3 (vi)]

Essentially all analytical work has focused on the 2D heat equation with no variations along the heater length (y direction), which clearly requires $L \gg \lambda_S$. This effect was quantified in a numerical study by Jacquot et al.[45] for two configurations of a line heater on a semi-infinite substrate. The most common is when the heater's electrical resistance is only measured over its central half by using voltage taps at $y = \pm L/4$, as shown in Fig. 1(a), in which case the results showed that the infinite heater assumption causes $<$1% error in the temperature as long as $L/\lambda_S > 4.7$. A second configuration is when the heater resistance is measured over its full length from $-L/2$ to $+L/2$, which requires a somewhat longer heater ($L/\lambda_S > 15$ to keep errors to $<$1%).[45] Therefore, the former configuration is always recommended.

3.9 Maximum Frequency to Neglect the Heat Capacity of Heater [Table 3 (vii)]

Simple expressions for the effect of the heater's heat capacity were obtained by Ju and Goodson[44] and Borca-Tasciuc et al.,[42] who both found that the errors are approximately

$(C_H/C)\,(d_H d/\lambda^2)$, where C is the volumetric heat capacity. As noted above, usually λ/d, and it is often the case that the heater is much thinner than the film $(d_H \ll d)$. Also, around room temperature and above, C for a large range of fully dense materials does not vary by more than a factor of two from $\sim 2 \times 10^6$ J/m^{3}K, reflecting the DuLong and Petit heat capacity result and relatively invariant atomic concentration.[48,49] Thus, the errors due to the heater's heat capacity should usually be tolerably small. However, care should be taken if the film is particularly thin, and if the measurements include cryogenic temperatures it may be beneficial to select a heater with a high Debye temperature to help minimize C_H at low T. (On the other hand, by intentionally pushing the measurement to high frequencies, the 3ω method has also been used to measure $C_H d_H$).[50]

3.10 Heater as Uniform Q or Uniform T [Table 3 (viii)]

Nearly all 3ω analyses approximate the heater line as a uniformly distributed heat source, thereby neglecting any in-plane heat spreading within the heater. This issue has received little quantitative attention, although it has been appreciated from the earliest work[3,11] and commented on in Refs. 45 and 47. We now use the results of Section 3.4 to quantify the likely bounds of this error, and show that the error is never overwhelming and often may be simply neglected.

Figure 6(a) shows the two limiting solutions, for the heater as a uniform heat source[42] and as a uniform T source,[43] both assuming an isothermal substrate. The two solutions converge in the narrow and wide heater limits. For intermediate heater widths, $(b/d)(k_z/k_x)^{1/2} \sim 1$, the thermal resistance for the uniform-T heater is slightly smaller than that of the uniform-Q heater. Physically, this is because the isothermal heater redistributes the heat preferentially near the heater edges, where per unit dx of heater width there is increased solid angle for conduction through the film, thus lowering the effective R_F.

The worst-case difference between the two bounds is never more than 6.4%, and is less than 3% as long as $(b/d)(k_z/k_x)^{1/2} < 0.06$ or $(b/d)(k_z/k_x)^{1/2} > 4.8$. Because this last wide-heater condition should already be satisfied for a 1D cross-plane measurement [Table 3 (ii)], we can conclude that the additional complication of distinguishing between isothermal and constant-Q heaters should be unimportant for properly designed measurements of k_z.

In the intermediate regime, which is important for the variable-linewidth 3ω method, $(b/d)(k_z/k_x)^{1/2} \sim 1$, and the following scaling argument can be used to choose between the two heater models. A characteristic resistance for heat spreading within the heater line is $b/2k_H d_H L$, whereas that for 1D heat flow across the film is $d/2kbL$. Thus, a criterion to neglect heat redistribution within the heater line is $(d_H d/b^2)(k_H/k) \ll 1$. Plugging in typical numbers suggests that this criterion is often satisfied, in which case the constant-Q heater solutions again are well justified.

4. INSTRUMENTATION AND HARDWARE ISSUES

The most common circuit used for 3ω measurements of films is shown in Fig. 7. Briefly, a sinusoidal current source provides a pure 1ω current, which causes 2ω heating, leading

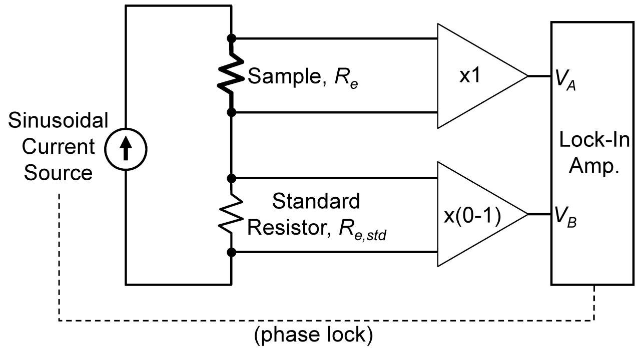

FIG. 7: The most common electrical connections used for 3ω measurements, facilitating subtraction of the large 1ω background voltage. Variations are described in the main text.

to the 3ω voltage discussed above [Fig. 2(b)]. However, the 1ω voltage drop across the sample is typically 100–1000 times larger than the 3ω voltage [by a factor of $2/\alpha\theta_{2\omega}$, see Eq. (10)], so it is common practice to use a simple subtraction circuit to remove most of this 1ω background. The rest of this section is devoted to selected practical details about this measurement configuration. Although presented here in the context of a cross-plane 3ω measurement, many of these issues are also relevant for in-plane 3ω measurements, 3ω measurements of a substrate's k_S,[11] and DC methods.

4.1 Current Source

There are three basic strategies to create a sinusoidal current source. At present, the most convenient is to use a commercially available AC source (e.g., Keithley 6221A) phase locked to the lock-in amplifier.[32,39,51] Another good option is to combine a home-built V-to-I circuit with a standard sinusoidal voltage source,[52] such as a function generator or the lock-in amplifier's own voltage source. Finally, the simplest approach is to use the lock-in's voltage source in series with a "ballast resistor" to approximate a current source.[53–56] This approximation is only appropriate if the sample resistance is much smaller than the ballast resistance. Otherwise, a correction factor is available,[17] although it should not be applied[57] if electrical background subtraction is in use, as in Fig. 7. Although unlikely, in the opposite extreme where the sample's electrical resistance dominates all others, an alternative strategy would be to use a pure 1ω voltage source and measure the 3ω current.[17]

4.2 Voltage Measurement and Subtraction of 1ω Background

In almost all cases, the 3ω voltage is measured with a commercial lock-in amplifier, although it has also been shown possible to digitize the voltage waveform directly and perform the equivalent signal processing in software.[54] Various modern lock-in amplifiers can conveniently detect the third harmonic voltage, removing the need for a frequency tripler subcircuit used in early work.[11]

The 1ω background subtraction is most commonly performed as indicated in Fig. 7, following the original scheme of Cahill.[11] Typically, the standard resistor $R_{e,\mathrm{std}}$ is an adjustable potentiometer or resistance decade box, with low temperature coefficient of resistance α and low thermal resistance to the environment to minimize any spurious 3ω artifacts. In one approach, the value of $R_{e,\mathrm{std}}$ is adjusted manually for every sample and temperature of interest to closely match the corresponding value of the sample's electrical resistance R_{e0}, in which case the amplifier driving V_B can simply have a unity gain. Alternatively, at the start of a set of experiments, $R_{e,\mathrm{std}}$ can be manually set once to a value slightly higher than the largest expected value of R_e, and then the amplifier driving V_B is placed in series with a multiplying digital-to-analog converter, which is equivalent to a variable gain element from 0 to 1.[11,53] In this case, a computer is used to vary the gain at every temperature of interest so that (gain) $\times\ R_{e,\mathrm{std}} \approx R_{e0}$, making the differential signal $V_A - V_B$ nearly free of the 1ω background. A related variation is to use a Wheatstone bridge[50,58] to remove the background.

A less common option is to forgo the standard resistor and background subtraction entirely, instead relying on the lock-in amplifier's dynamic reserve to detect the small 3ω signal in the presence of the much larger 1ω background.[17,52] This approach simplifies the circuitry but requires critical attention to the lock-in amplifier's gain and dynamic reserve settings. For example, if the 1ω background is $1000\times$ larger than the 3ω voltage, the dynamic reserve must be at least 60 dB. This is practical with modern lock-ins based on digital signal processing, which have stated reserves exceeding 100 dB. It should also be practical with the direct digitization approach[54] if the bit depth is sufficient (e.g., 24-bit digitization corresponds to a generous 144 dB of dynamic range, although this must accommodate both dynamic reserve and signal resolution).

The standard practice is to perform a frequency sweep at a fixed current, as suggested in Fig. 3(c). In experiments requiring the utmost accuracy, it may also be helpful to perform a current sweep at one or more fixed frequencies, and focus on obtaining the *derivative* $\partial(V_{3\omega})/\partial I_{1\omega}^3$ with the best possible accuracy.[32,59] This derivative is closely related to $\partial T_H/\partial Q$, and can be contrasted with the traditional approach of Eqs. (8), which evaluates the *ratio* $V_{3\omega}/I_{1\omega}^3$. In an ideal measurement, the derivative and ratio are equal. But the derivative approach offers the potential advantage of being insensitive to any offset or related errors in $V_{3\omega}$ or $I_{1\omega}$. It has been used to measure thermal resistances with a repeatability of around $\pm 0.2\%$.[59] If applied to the traditional 3ω method of Eq. (13) to obtain k_S of a semi-infinite substrate, this derivative strategy leads to a "slope-of-slopes" expression

$$\frac{\partial\left[\partial(V_{3\omega})/\partial(I_{1\omega}^3)\right]}{\partial\ln(\omega)}$$

4.3 Resistance Thermometry

For electrothermal measurements from room temperature down to $\sim$50 K, the resistance versus temperature curve of most microfabrication-friendly metals such as Au, Pt, and Al is very linear, $R_e(T) \approx a_0 + a_1 T$, which is particularly convenient for resistance thermometry. The temperature coefficient of resistance (TCR) α for these metals is typically a few parts per thousand per Kelvin around room temperature. However, it is essential to calibrate each heater's TCR because the value for metallic thin films will be substantially lower (a factor of two is not unusual) than the handbook values, due to increased scattering of electrons by film surfaces and grain boundaries.[60] Referring to the 3ω equations [Eq. (6)], it is also convenient to recognize that α always appears as the product $\alpha R_{e0} = dR_{e0}/dT$, because dR_{e0}/dT often has a weak to negligible T dependence even though α and R_{e0} each have strong T dependencies. Strain gauge effects on R_e are almost universally neglected, which may be justified because α is typically $\sim 100\times$ larger than the mismatch of thermal expansion coefficients between most heater and substrate pairings. With their much larger expansion coefficients, polymeric substrates may be an exception, and indeed strain gauge effects were identified as a consideration for high-accuracy 3ω measurements of polymethyl methacrylate (PMMA) composite substrates.[61]

Below about 50 K, the $R_e(T)$ curves for these pure metals flattens out, gradually deviating from the linear approximation and ultimately becoming completely flat as $T \to 0$ K. Incorporating these nonlinearities into the $R_e(T)$ curve allows the practical range of resistance thermometry to be pushed down to perhaps 20–30 K. This is sometimes done by approximating $R_e(T)$ with a higher-order polynomial, or as piecewise linear or piecewise parabolic. A more physically satisfying fit for $R_e(T)$ uses a simple three-parameter Bloch-Grüneisen model to cover the entire range from 0 K to above room temperature.[32,61,62]

For sensitive resistance thermometry below ∼20 K, pure Au, Pt, and Al are not useful and alternative heater materials are required. The Kondo effect of magnetic impurity scattering may be exploited in this regime, which gives a negative dR_e/dT below ∼20 K for Cu or Au alloyed with <1% Fe. However, the downside is a regime of vanishing sensitivity at the minimum in the $R_e(T)$ curve, typically located around 20–30 K.[49] Although uncommon in microfabrication, Rh alloyed with less than 1% Fe has a more convenient $R_e(T)$ curve with positive dR_e/dT continuously from room temperature to <1 K,[63] and has been applied for related thermal measurements.[27] Other alternative materials with good low-temperature TCR characteristics that may be amenable to heater microfabrication include ZrN_x,[64] Si doped with Nb,[65] and doped Ge.[63,66]

For high-temperature measurements above ∼400 K, the challenge becomes the stability of the metal heater films, whose resistance drifts as they gradually anneal during an experiment. Among the most common metals, Al is apparently less sensitive than Au and Pt to this annealing instability, which can be overcome by pre-annealing the films for an hour at a temperature somewhat higher than the maximum intended measurement temperature.[11,67]

4.4 Helpful Checks

Novices approaching a 3ω measurement for the first time might be well served by first measuring a thick substrate ($d_S \geq 1$ mm) of low thermal conductivity without a film, such as amorphous SiO_2, to ensure that the signals and data processing behave as expected. The advantage of measuring a low-k_S substrate is that the signals will be much stronger [see Eqs. (8) and (13)]; however, when a film is measured, the substrate should of course be chosen with high k_S, to ensure that most of the temperature drop occurs across the film. In the initial stages of a new effort, it is advisable to confirm that the 3ω voltages scale with the cube of the 1ω current, and that the frequency dependence of $V_{3\omega,\text{rms,in-phase}}/I^3_{1\omega,\text{rms}}$

follows the form of $-\text{const} + \ln(\omega)$ as expected from Eqs. (8) and (13)[17] (note that it is common practice to omit the sign and plot the absolute value of these quantities). Various difficulties such as poor connections or suboptimal lock-in settings may be identified through these checks.

5. IN PLANE: SUSPENDED FILMS

The electrothermal methods used to measure the in-plane thermal conductivity of films are considerably more diverse than those used for cross-plane measurements. Two techniques for suspended films are described in this section, and two for supported films in Section 6. Another electrothermal method not discussed below uses more extensive microfabrication to create two suspended platforms.[68,69] In general, the supported techniques have easier sample fabrication, but have more restrictions about their domain of validity and are inherently less sensitive. The suspended samples are much more vulnerable to convection and radiation losses, and must be measured in vacuum. Many of the instrumentation and hardware issues are similar to those already discussed in Section 4.

5.1 Central Line Heater Method

Figure 8 shows arguably the most common and accurate method for measuring the in-plane thermal conductivity of films, although it is also the most demanding for sample fabrication. A suspended film is patterned with a metallic line heater near its center that also acts as a temperature sensor. Representative dimensions are w = 500 μm, L = 5000 μm, and d = 1 μm. AC or DC joule heating Q enters the film and flows one-dimensionally in the x direction until it reaches the supporting substrate, at which point the heat can spread both laterally $(x - y)$ and vertically (z) down into the substrate. Accounting for the symmetry around the $y - z$ plane and neglecting radiation and convection losses, the film thermal conductivity is given simply by the 1D conduction result,

$$k = \frac{Qw}{2dL\,(T_{F,1} - T_{F,2})} \tag{19}$$

As summarized in Table 1, this method has been used to measure a variety of low- and high-thermal conductivity films, including polymers, Si, and diamond. Besides the self-evident microfabrication challenges, successful implementation of this method requires attention to radiation losses, thermal contact and spreading resistances, and other issues, discussed below in Sections 5.3–5.6.

5.2 Variation: Distributed Self-Heating Method

If the film of interest is electrically conducting with a stable $I - V$ curve, such as a metal, rather than incorporating an extra dielectric layer between film and heater, it is more convenient to use the film itself as both heater and temperature sensor [Figs. 9(a) and 9(b)]. Sufficient electrical current is passed through the suspended portion of the film to cause measurable self-heating. For metallic bridges near room temperature, a helpful rule of

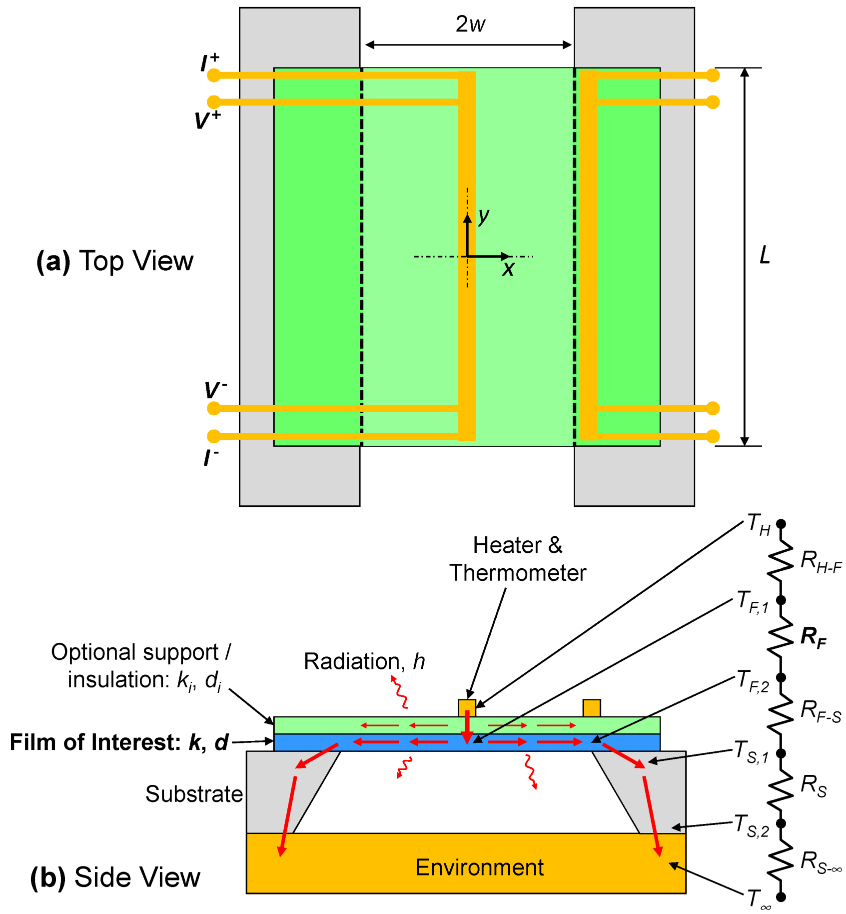

FIG. 8: The central line heater method to measure the in-plane thermal conductivity of a suspended film.

thumb due to the Wiedemann-Franz law is that the temperature rise due to self-heating is approximately $\langle T_F \rangle - T_{F,2} \approx (1\,\mathrm{K})\,(V/9.4\,\mathrm{mV})^2$, where $\langle T_F \rangle$ is the average film temperature within $-w < x < w$, and this result is independent of the film's L, w, d, and resistivity.[59] Neglecting radiation losses, the heat conduction equation is easily solved to give a parabolic temperature profile $T_F(x) = -(Q/4wLdk)(x^2 - w^2) + T_{F,2}$, where $Q = I\,(V^+ - V^-)$ is the power dissipated in the suspended portion of the film. Four-probe resistance thermometry as indicated in Fig. 9(a) gives $\langle T_F \rangle$, which after averaging $T(x)$ is

$$\langle T_F \rangle = T_{F,2} + \frac{Qw}{6Ldk} \tag{20}$$

thus allowing k to be determined. This method can also be adapted to measure k of electrically insulating films if they can be coated with a metal layer of known properties [Fig. 9(c)].[1]

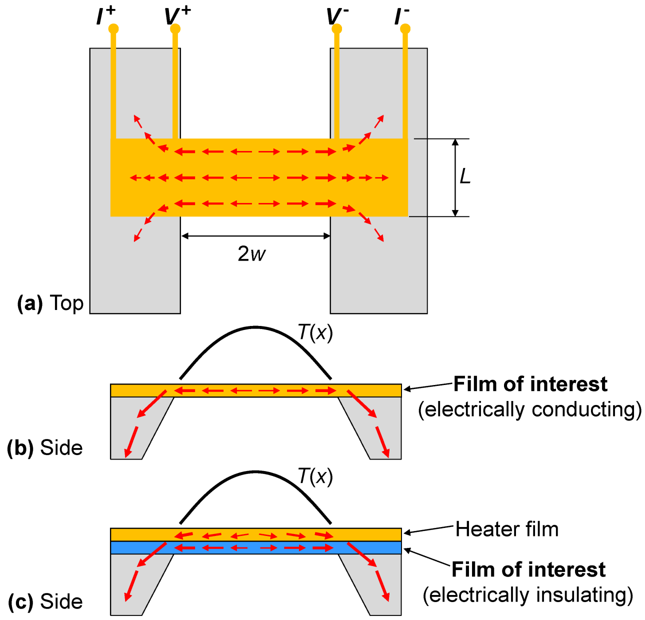

FIG. 9: The distributed self-heating method to measure the in-plane thermal conductivity of a suspended film. (a,b) Metallic film. (c) Variation to measure an electrically insulating film. The shape and placement of the electrical leads can be important in this method (see Fig. 11).

5.3 Radiation Losses

Even after placing the samples in high vacuum to eliminate convection, the radiation losses from the upper and lower surfaces are a critical consideration for suspended films. The impact of the losses can be estimated as the ratio of $Q_{\mathrm{rad}}/Q_{\mathrm{cond}}$. For simplicity, here we use the linearized radiation coefficient from Eq. (14), and assume the linear $T_F(x)$ conduction solution corresponding to Fig. 8 is correct to leading order. Thus, $Q_{\mathrm{cond}} = 2kLd(T_{F,1} - T_{F,2})/w$ and $Q_{\mathrm{rad}} = 4h_{\mathrm{rad}}wL[(1/2)(T_{F,1} + T_{F,2}) - T_\infty]$, so

$$\frac{Q_{\mathrm{rad}}}{Q_{\mathrm{cond}}} \approx \frac{2h_{\mathrm{rad}}w^2\left[(1/2)\left(T_{F,1} + T_{F,2}\right) - T_\infty\right]}{kd\left(T_{F,1} - T_{F,2}\right)} \tag{21}$$

If we further assume that the radiative surroundings T_∞ are at nearly the same temperature as $T_{F,2}$,

$$\frac{Q_{\mathrm{rad}}}{Q_{\mathrm{cond}}} \approx \frac{h_{\mathrm{rad}}w^2}{kd} \tag{22}$$

which is also equal to $(1/2)(\beta w)^2$, where as usual the fin parameter is $\beta = \sqrt{2h_{\mathrm{rad}}/kd}$.[21] A further complication is that h_{rad} depends on the emissivity of the film, ε, which is generally unknown. Allowing for the worst case of h_{rad} = 6.1 W/m^{2}K at 300 K, a film with d = 1 μm, w = 500 μm, and k = 150 W/m K (e.g., Si) would have a very reasonable

$Q_{\rm rad}/Q_{\rm cond} \approx 1\%$, but if that same film were made out of an insulator with $k = 1$ W/m K, the radiation losses would be completely unacceptable.

The best way to deal with radiation losses is to choose w such that $Q_{\rm rad}$ is negligible even for the worst case of $\varepsilon = 1$.[26,70–72] If it is desired to determine ε as well, an extension is to prepare additional samples with larger w, and/or vary the radiation bath temperature T_∞, thereby deliberately obtaining data with non-negligible $Q_{\rm rad}$.[73,74] Another variation is to measure $T(x)$ at multiple points along the film surface, which when combined with the related radiation fin equations allows both k and ε to be obtained.[75]

5.4 Contact and Substrate Spreading Resistance

The contact and spreading resistance from the film edge to the environment is another important consideration. In terms of Fig. 8, this is $R_{F-\infty} \equiv R_{F-S} + R_S + R_{S-\infty}$. As suggested in Fig. 8, the ideal solution is to include a dedicated temperature sensor to measure $T_{F,2}$.[71] If, for convenience of fabrication, this sensor is omitted and $T_{F,2}$ approximated as T_∞, it is important to estimate the intervening resistances to ensure they are negligible.[1,70,73,76] Note the competing demands on w. To neglect $T_{F,2} - T_\infty$ in comparison with $T_{F,1} - T_{F,2}$ one should increase w to make R_F as large as possible, but as noted above this will also increase the radiation losses. One convincing way to demonstrate $T_{F,2} - T_\infty$ is negligible would be to measure several samples with different w. This is very similar in spirit to the differential 3ω method, and a plot analogous to Fig. 4(b) (right) could also be used to estimate $R_{F-\infty}$ if it were not actually negligible.

AC heating methods[26] have been infrequently applied for membrane measurements, but offer the potential benefit of localizing the oscillating temperature field within the membrane and thereby reducing sensitivity to $R_{F-\infty}$. This is closely analogous to one of the benefits of AC heating in the cross-plane 3ω method. However, as noted above in Section 3.2, these other series resistances still affect the background DC temperature rise. Also, transient measurements in a planar geometry may be less convenient because they fundamentally yield the thermal diffusivity k/C or effusivity $\sqrt{kC}$, rather than purely k itself.[26,73,74]

The contact resistance between the heater and film is commonly neglected, which can be justified by estimating $R_{H-F} = R_c''/2bL$ in comparison with R_F, where as noted above typical R_c'' between metals and dielectrics are $\sim 10^{-8}$–10^{-7} m^{2}K/W.[22,23] However, if the film has particularly high k (small R_F), and/or a low-conductivity dielectric layer is included between heater and film as suggested in Fig. 8(b), its contribution to R_{H-F} is likely to be substantial and cannot be neglected. In this case, it may be necessary to place another temperature sensor in close proximity to the heater.[72,77,78]

5.5 Effect of Multiple Layers

As indicated in Figs. 8(b) and 9(c), for measurements of suspended films, it is not uncommon to incorporate additional layers besides the film of interest, for example, for mechanical support, electrical insulation, or as a distributed heat source.[1,71–74,78] In this case, it is clear that the layers in the stack all contribute to the in-plane heat transfer weighted by their kd product. Far away from the heater and substrate, there is no concern about temperature gradients in the z direction because the thickness Biot number, Bi $= h_{\text{rad}}\Sigma\,(d/k)$, will always be negligible, due to the micron-scale values of d.

5.6 2D Spreading Effects

Although Figs. 8 and 10(a) show a suspended film with free edges at $y = \pm L/2$, to facilitate microfabrication, sometimes the film is anchored at all four edges, as indicated in Fig. 10(b). In this case, it is clear that the heat flow in the membrane will be 2D rather than 1D as assumed in Eq. (19). For films with $L/w \gg 1$, the edge effects can be neglected for small y, which is readily exploited by placing the voltage taps to measure the temperature only near the center of the film [Fig. 10(b)].[26,72] Alternatively, the 2D conduction equation can be solved for the average T from $-L/2$ to $+L/2$.[73,76] For very low-conductivity films, the heat losses through the heater leads may also be important.[26]

5.7 Placement of Voltage Probes

For the self-heated method of Fig. 9, the aspect ratio $2w/L$ (equivalent to the number of squares of sheet resistance for the suspended portion) is not always large, typically around 10–20,[1,70,79] and sometimes only $\sim$1.[75] In this case, the placement of the voltage probes requires some attention. Figure 11 summarizes numerical calculations for five representative configurations of suspended films.[3] In all cases, the absolute errors expressed as numbers of squares are essentially independent of w (holding all other dimensions constant), allowing these calculations to be adapted to some other configurations not shown.

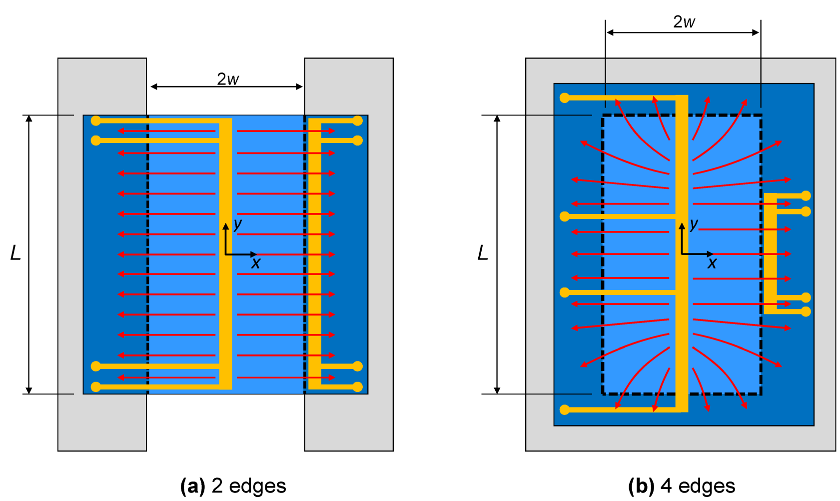

FIG. 10: Edge effects and the central line heater method. (a) Best case, supported on two edges (same as Fig. 8). (b) Supported on all four edges, distorting the heat flow away from being purely 1D. Note the placement of the current and voltage leads for the heater and edge T sensor in (b).

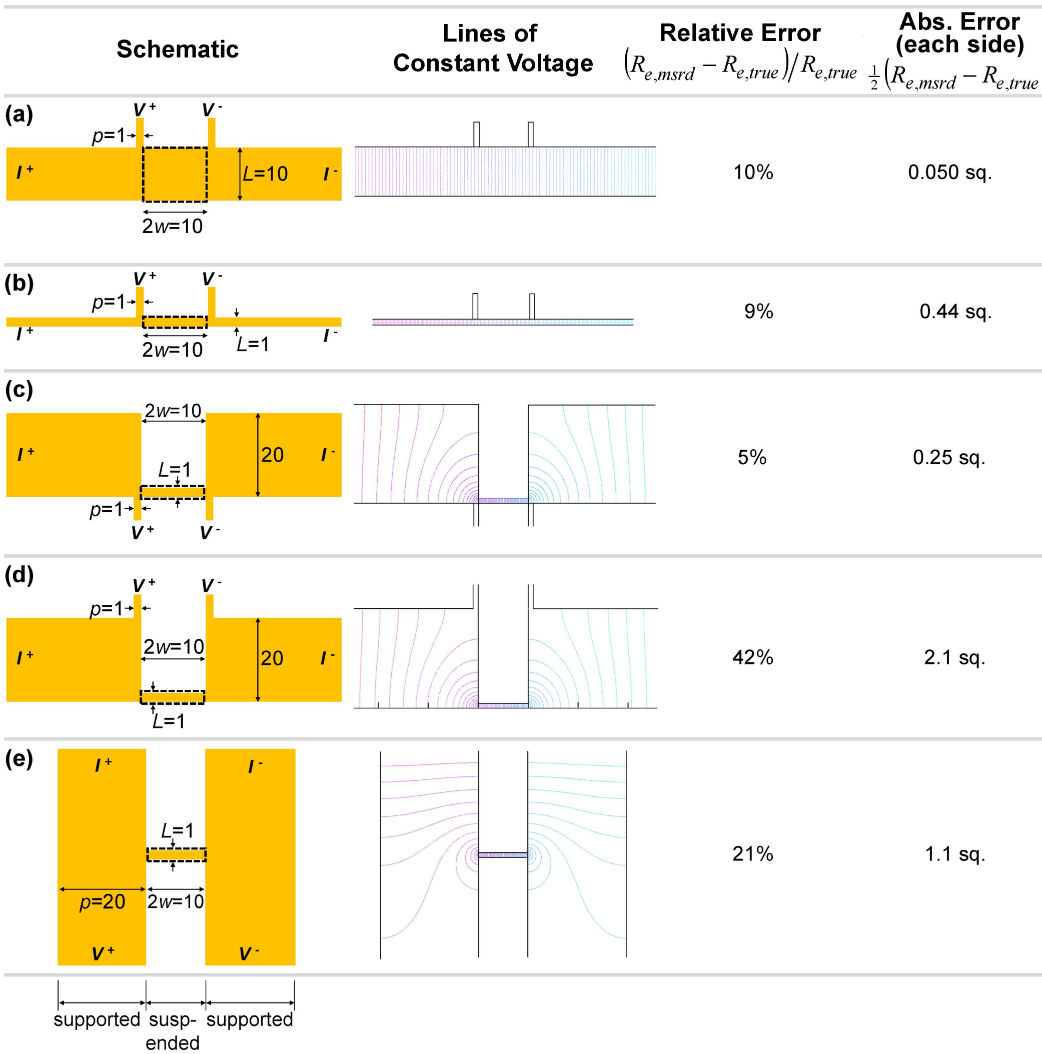

FIG. 11: Examples of five possible configurations for placing the voltage probes to measure R_e in the distributed self-heating method of Fig. 9. In all cases, the suspended test section is indicated by the dashed line, and the definitions of L and w are consistent with Fig. 9. The number of squares ($2w/L$) in the test section in (a) is one, while all others have 10 squares. Configuration (c) gives the most accurate measurements of R_e for the distributed self-heating method. [Although Fig. 11 emphasizes suspended films, configuration (b) is also commonly used for cross-plane 3ω measurements of supported films like Fig. 1. In this case, Fig. 11(b) shows that the effective heater length determining R_e should be increased by $2b\times$ 0.88 compared to the nominal length between the inside edges of the voltage probes, usually a very minor correction.]

Figure 11 shows that contact configuration (c) will have the smallest relative errors in determining R_e for the distributed self-heating method, followed closely by (b) and (a).

Configurations like (d) have also been used,[79] although the errors are substantially larger than (c). The electrical errors in (e) are about four times larger than (c). However, if the supporting substrate exists only under the metal pads [unlike Fig. 9(a) where the supporting portions of the substrate extend to $\pm\infty$ in y], configuration (e) has the advantage that its thermal R_{F-S} + R_S should be only half as large as that for (c). Such a configuration sometimes arises if the microfabrication ends with a sacrificial release etch. In this case, choosing between configurations (c) and (e) requires a detailed estimate of the electrical and thermal resistances near the contacts.

The R_e accuracy of all but configuration (d) can be further improved by reducing the voltage probes' linewidth p, as lithography permits. For arrangements like (a) and (b) where the test section is simply a continuous segment of the I^+/I^- leads with the same cross section, the absolute error at each side, expressed in squares, is approximately $p/2L$ (exactly so in the limit $p \ll L$). Configurations (c)–(e), on the other hand, all exhibit 2D radial spreading resistances around the transition from the narrow test section to the much larger I^+/I^- lines. In this case, the absolute error is expected to scale as ln$(p/2L)$ if $p \gg L$, while becoming independent of p for $p \ll L$.

6. IN PLANE: SUPPORTED FILMS

For certain types of films, the microfabrication of large-area suspended samples is inconvenient or even impossible. In this case, alternative techniques for measuring the in-plane k of supported films are an important option, although the resulting measurements will generally be less sensitive and harder to interpret than the method of Fig. 8. Below, we describe two such techniques: the variable-linewidth 3ω method and the heat spreader method.

6.1 Variable-Linewidth 3ω

6.1.1 Basic Concept

The cross-plane 3ω method detailed in Sections 2 and 3 emphasizes wide heaters such that the heat flow was almost perfectly 1D in the z direction, making the measurement sensitive only to the film's k_z. However, as shown in Fig. 6, it is possible to exploit the opposite extreme of large in-plane heat spreading to determine k_x.[26,43,80] The narrow-heater regime can be defined as $(b/d)(k_z/k_x)^{1/2}$ of ~0.1 or less. In this case, the thermal resistance R_F is sensitive to both k_x and k_z, so it is standard practice to prepare a second heater of much greater width to independently obtain k_z. Greater accuracy could be achieved by measuring a series of multiple heater widths and fitting the observed $R_F(b)$ data to Eq. (16), as in Fig. 6(a). If numerical evaluation of Eq. (16) is deemed inconvenient, the domains of validity of Eqs. (17) and (18) conveniently overlap, so a simplified expression with better than 3% accuracy is always available.

6.1.2 Sensitivity

An important weakness of the variable-linewidth 3ω method is that it is inherently less sensitive to k_x as compared to the suspended methods. This can be quantified using the results of Section 3.4. Even in the limit of a very narrow heater line, we see from Eq. (18) that R_F goes very nearly as $k_x^{-1/2}$, so that a 10% change in k_x causes at best only a 5% change in R_F; and obviously in the limit of a wide heater line R_F is not sensitive to k_x at all. We define the dimensionless sensitivity in the usual way as –[∂ln$(R_F)/\partial$ln$(k_{x,z})$], where the negative sign is introduced here because increasing k always reduces R_F. The sensitivity for Eq. (16) is shown in Fig. 6(b), which shows that even for a relatively narrow heater of $(b/d)(k_z/k_x)^{1/2} \sim 0.1$, the sensitivity of R_F to changes in k_x is only ~0.35 (e.g., increasing k_x by 10% would reduce R_F by only 3.5%). In contrast, for the two methods presented above for suspended films, the sensitivity of R_F to changes in k_x is simply 1.

6.1.3 Conditions for the Variable-Linewidth 3ω Method to be Appropriate

- Lithography permits narrow enough linewidths to achieve $(b/d)(k_z/k_x)^{1/2} < 0.1$, ensuring the sensitivity to k_x is better than 0.35.
- Even if only k_x is of interest, k_z must also be known or measured with high accuracy. Recall from Eqs. (16)–(18) that R_F depends on both k_x and k_z. In particular, Eq. (18) and Fig. 6(b) show that any uncertainty in k_z is magnified in k_x; for example, at $(b/d)(k_z/k_x)^{1/2} = 0.1$, a 10% error in k_z would cause a 19% error in k_x, while at $(b/d)(k_z/k_x)^{1/2} = 1$, a 10% error in k_z would cause a 56% error in k_x.
- The substrate thermal conductivity is high enough to be approximated as isothermal. For an anisotropic film, Borca-Tasciuc et al.[42] showed that the substrate contrast criterion of Table 3 (i) generalizes to Error $\approx (k_x k_z/k_S^2)$. This criterion means that the variable-linewidth 3ω method is generally not applicable to measure films with high in-plane thermal conductivity, such as graphene. In this case, the heat spreader method described in Section 6.2 is more appropriate.

6.2 Heat Spreader Method

The basic concept of the heat spreader method is shown in Fig. 12. The film of interest should have high in-plane thermal conductivity and is supported by a thin insulation layer on a high-thermal conductivity substrate. Joule heating from the heater line flows into the film of interest, which, acting as an effective heat spreader, moves the heat laterally. At the same time, the heat also bleeds gradually downward into the isothermal substrate. Thus, by measuring the nearby temperature distribution, it is possible to extract the in-plane thermal conductivity of the film of interest.

Because of the complexity of fabrication and interpretation, this heat spreader method is less common than the variable-linewidth 3ω method, but may prove useful when the latter cannot be applied. A good example is found in the measurements of the in-plane thermal conductivity of encased graphene and ultrathin graphite in Ref. 2. For representative values $k_x \approx 300$ W/m K, $k_z \approx 6$ W/m K, and $d \approx 0.003$ μm, to ensure adequate sensitivity to k_x, the variable-linewidth 3ω method would require heater linewidths $2b < 0.004$ μm, which is completely impractical for lithography. Also very importantly, the contact resistance R_c'' between graphite and substrate is likely to be $\sim 10^{-8}$ m^2 K/W,[32] which is nowhere close to

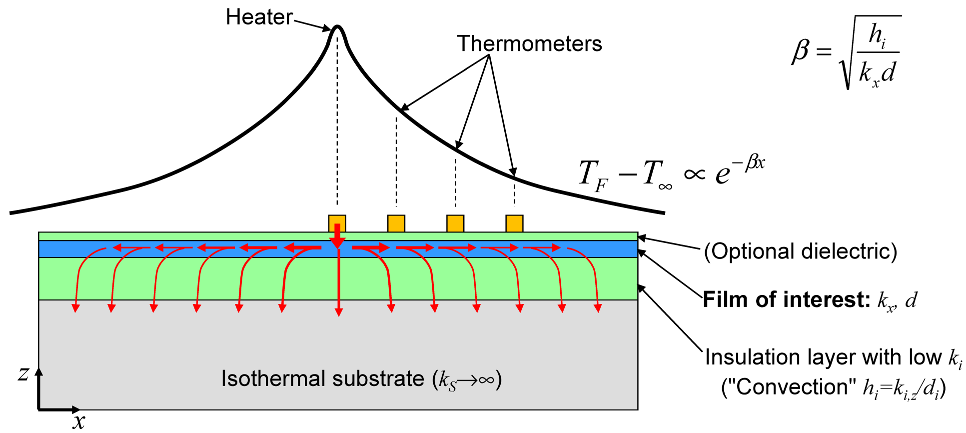

FIG. 12: A heat spreader method to measure the in-plane thermal conductivity of a supported film. Joule heating from the line heater is spread laterally by the high-k film of interest, while at the same time leaking vertically through the low-k insulation layer. For sufficiently small values of the fin parameter β, the temperature profile in the film obeys the classical fin equation, decaying exponentially in x.

negligible compared to the cross-plane film resistance $d/k_z \sim 5 \times 10^{-10}$ m^2 K/W, making it impossible to apply the usual 3ω analyses of Section 3.4.

Returning to Fig. 12, we recognize that this heat spreader system is analogous to the classic fin problem from elementary heat transfer, where the "fin" is the film of interest and the "convection coefficient" arises from the cross-plane conduction through the insulating film: $h_i = k_{i,z}/d_i$. Because h_i is typically of order ~10^6 W/m^2 K (1 μm film of SiO_2), any additional air convection or radiation to the surroundings should be negligible. The additional thermal contact resistances between film and insulator, and between insulator and substrate, should also be incorporated into h_i if known, but are usually negligible in comparison.

Following the well-known solutions for long fins,[21] the temperature profile in the plane of the film is ideally

$$T_\mathrm{F}(x) - T_\infty = \frac{Q}{2L}\sqrt{\frac{d_i}{k_{i,z}k_x d}}\; e^{-\beta x} \tag{23}$$

where now the fin parameter is given by $\beta = \sqrt{k_{i,z}/k_x d d_i}$. In this context, the characteristic fin length

$$\beta^{-1} = \sqrt{\frac{k_x d d_i}{k_{i,z}}} \tag{24}$$

is also known as the thermal healing length.[81] Thus, by measuring the temperature profile at several x locations, it is possible to fit for β, and finally obtain k_x.

Note carefully that Eqs. (23) and (24) are only sensitive to the *in-plane* thermal conductivity of the film (k_x) and the *cross-plane* thermal conductivity of the insulation layer

$(k_{i,z})$. To understand the physical significance of this distinction, it is helpful to compare β^{-1} of Eq. (24) with the related thermal spreading distance for a single film on an isothermal substrate (Fig. 5), which we see from Eq. (17) is of order

$$\sqrt{\frac{k_x d^2}{k_z}} \tag{25}$$

Comparing Eqs. (24) and (25) reveals that the fundamental effect of the underlying insulation layer in Fig. 12 is to decouple the dominant modes of heat transfer in the x and z directions: the in-plane conductance is controlled by the film of interest $(k_x d)$, while the out-of-plane conductance is controlled by the extra insulation layer [$k_{i,z}/d_i$ in Eq. (24)]. In contrast, in the variable-linewidth 3ω method of Fig. 5, both the in-plane $(k_x d)$ and out-of-plane (k_z/d) conductances are controlled by the film.

This decoupling allows much greater control over the length scale of in-plane heat spreading. Referring back to the example for ultrathin graphite,[2] even if the sample flake could somehow be deposited directly on an isothermal substrate with negligible contact resistance, the spreading length of Eq. (25) is only 0.02 μm. However, if that same graphite flake is deposited as a heat spreader on an insulating film with $k_{i,z}$ = 1 W/m K and d_i = 0.3 μm, the thermal healing length increases over 20-fold, to $\beta^{-1} \approx 0.5$ μm, a length scale now plausibly accessible by electron-beam lithography.[2]

The fin analogy of Eqs. (23) and (24) is only valid in limited circumstances. The thermal healing length β^{-1} must be much larger than the film thickness $d_i + d$ to justify approximating the heat conduction in the insulator as quasi-1D in z. The healing length should also be at least as large as the sensor pitch, and substantially larger than the sensor width (all in the x direction). These conditions were satisfied in the study of silicon films on SiO_2 insulation with a Si substrate (i.e., an SOI wafer) by Asheghi et al.,[81] with representative values $k \approx 100$ W/m K, $k_i \approx 1$ W/m K, $d \approx 1$ μm, and $d_i \approx 3$μm, corresponding to $\beta^{-1} \approx 17$ μm. The authors used numerical solutions of the 2D conduction equation to confirm that this healing length was acceptably large compared to the other length scales. In the more recent study of ultrathin graphite,[2] the submicron values of β^{-1} were not large enough to justify the fin Eqs. (23) and (24). Instead the authors used finite element methods to analyze the 3D heat conduction problem, and validated the analysis with a control experiment on a metal film of known k_x.

7. SUMMARY AND RECOMMENDATIONS

This chapter has presented the major electrothermal methods for measuring the thermal conductivity of thin films in both cross-plane and in-plane directions. Several highlights and recommendations are given below, and representative studies are summarized in Table 1.

7.1 Cross Plane

The 3ω method now appears to be widely accepted as the preferred electrothermal technique for measuring the cross-plane thermal conductivity of films, for good reason. As an AC technique, the 3ω method has advantages over DC techniques in determining or eliminating the thermal resistances of the substrate and its contact to the surroundings, and should also give more stable electrical measurements.

Cross-plane measurements are easiest for low-k films that are relatively thick, to maximize R_F of Fig. 1(b). Other requirements for accurate 3ω measurements have been thoroughly documented in the literature, with the major criteria summarized in Table 3. Common points requiring attention include ensuring the heater line is wide enough to approximate the film conduction as 1D, ensuring the substrate is thick enough to be approximated as semi-infinite, and avoiding very high frequencies where the heat capacities of the film and/or heater matter.

The differential 3ω method of Figs. 3(c) and 4(b) is preferred when practical because it eliminates many potential sources of uncertainty, most notably the thermal resistances of: the substrate, whether semi-infinite or finite and even at very low frequencies; any intervening buffer or insulation layers, as long as they can be held constant; and the interlayer contact resistances. (Note that this requires a subtle assumption, because once the film is absent the nature of the contact resistances changes. It is usually assumed that $R_{H-F} + R_{F-S}$ remains constant even in the control case of no film, although as is apparent from Fig. 4(b) there are one fewer interfaces once the film is absent, and the mating materials are also different. This assumption should be acceptable for all but the thinnest, most conductive films.) However, as long as careful attention is paid to the issues of Table 3, accurate results are possible, even for a single-thickness measurement.

7.2 In Plane

Measurements of the in-plane thermal conductivity are less common than for the cross-plane direction, while the methods used are more diverse. In-plane measurements can be divided into those for suspended and supported films. In general, methods for suspended films are more sensitive, accurate, and flexible, but the microfabrication to suspend the film is sometimes a serious challenge.

Figures 8 and 9 show the major measurement methods for *suspended* films. The most important concern is making the film length ($2w$) long enough so that the spreading and contact resistances at substrate and heater can be neglected in comparison, but still short enough to ignore radiation losses and 2D effects due to finite L. Although these errors can in many cases be estimated satisfactorily, their (in)significance can also be checked experimentally by measuring several films with different w, and by including separate temperature sensors near the heater and the film-substrate junction.

Techniques for measuring the in-plane thermal conductivity of *supported* films are more specialized and include the variable-linewidth 3ω method (Figs. 5 and 6) and the heat spreader method (Fig. 12). Compared to the methods for suspended films, these supported methods are inherently less sensitive (signals scaling at best as $k_x^{1/2}$), so their primary appeal is the potentially simpler microfabrication. However, the need for relatively narrow and/or closely spaced heating/sensing lines must not be overlooked. Both supported methods work best for relatively thick films with high k_x, whereas their requirements for k_z differ substantially. The variable-linewidth 3ω method works best for films with small k_z, which must be known with high accuracy. On the other hand, the heat spreader method works best for films with moderate to large k_z, which drops out of the analysis completely if $d/k_z \ll d_i/k_i$. Finally, the error analysis in these supported configurations is relatively undeveloped in the literature, especially as compared to the cross-plane 3ω method (e.g., Table 3), and owing to the complexity of the samples may ultimately require numerical rather than analytical approaches.[2]

ACKNOWLEDGMENTS

The author thanks C. T. Harris and S. K. Yee for critical readings of the manuscript. This work was supported in part by the NSF (Grants No. CBET 0854554 and No. 1055317) and the DARPA/DSO NMP program (Grant No. W911NF-08-C-0058).

REFERENCES

1. W. Liu and M. Asheghi, Thermal conductivity measurements of ultra-thin single crystal silicon layers, *J. Heat Transfer*, **128**:75–83, 2006.
2. W. Jang, Z. Chen, W. Bao, C. N. Lau, and C. Dames, Thickness-dependent thermal conductivity of encased graphene and ultrathin graphite, *Nano Lett.*, **10**:3909–3913, 2010.
3. D. G. Cahill, M. Katiyar, and J. R. Abelson, Thermal-conductivity of alpha-SiH thin-films, *Phys. Rev. B*, **50**:6077–6081, 1994.
4. C. A. Paddock and G. L. Eesley, Transient thermoreflectance from thin metal films, *J. Appl. Phys.*, **60**:285–290, 1986.
5. P. M. Norris, A. P. Caffrey, R. J. Stevens, J. M. Klopf, J. T. McLeskey, and A. N. Smith, Femtosecond pump–probe nondestructive examination of materials (Invited), *Rev. Sci. Instrum.*, **74**:400–406, 2003.
6. D. G. Cahill, Analysis of heat flow in layered structures for time-domain thermoreflectance, *Rev. Sci. Instrum.*, **75**:5119–5122, 2004.
7. A. J. Schmidt, Pump–probe thermoreflectance, *Ann. Rev. Heat Transfer*, **16**:159–181, 2013.
8. S. Rohmfeld, M. Hundhausen, and L. Ley, Contactless measurement of the thermal conductivity of thin SiC layers, in *Silicon Carbide, Iii-Nitrides and Related Materials, Pts 1 and 2*, edited by G. Pensl, H. Morkoc, B. Monemar, and E. Janzen (Transtec Publications Ltd, Zurich-Uetikon), Vol. 264-2, pp. 657–660, 1998.
9. A. A. Balandin, S. Ghosh, W. Bao, I. Calizo, D. Teweldebrhan, F. Miao, and C. N. Lau, Superior thermal conductivity of single-layer graphene, *Nano Lett.*, **8**:902–907, 2008.
10. W. Cai, A. L. Moore, Y. Zhu, X. Li, S. Chen, L. Shi, and R. S. Ruoff, Thermal transport in suspended and supported monolayer graphene grown by chemical vapor deposition, *Nano Lett.*, **10**:1645–1651, 2010.
11. D. G. Cahill, Thermal conductivity measurement from 30 K to 750 K: The 3-omega method, *Rev. Sci. Instrum.,* **61**:802–808, 1990.
12. D. G. Cahill, H. E. Fischer, T. Klitsner, E. T. Swartz, R. O. Pohl, Thermal-conductivity of thin-films-measurements and understanding, *J. Vac. Sci. Technol. A-Vac. Surf. Films*, **7**:1259–1266, 1989.
13. K. E. Goodson and M. I. Flik, Solid layer thermal-conductivity measurement techniques, *Appl. Mech. Rev.*, **47**:101–112, 1994.

14. S. R. Mirmira and L. S. Fletcher, Review of the thermal conductivity of thin films, *J. Thermophys. Heat Transf.,* **12**:121–131, 1998.
15. T. Borca-Tasciuc, G. Chen, Experimental Techniques for Thin-Film Thermal Conductivity Characterization, in *Thermal Conductivity*, edited by Terry M. Tritt (Springer US), pp. 205–237, 2004.
16. D. G. Cahill and R. O. Pohl, Thermal conductivity of amorphous solids above the plateau, *Phys. Rev. B*, **35**:4067–4073, 1987.
17. C. Dames and G. Chen, 1 omega, 2 omega, and 3 omega methods for measurements of thermal properties, *Rev. Sci. Instrum.,* **76**:124902-1–124902-14, 2005.
18. D. G. Cahill, Erratum: Thermal conductivity measurement from 30 to 750 K: The 3 omega method (*Rev. Sci. Instrum*, **61**:802–808, 1990), *Rev. Sci. Instrum.,* **73**:3701–3701, 2002.
19. J. Y. Duquesne, D. Fournier, and C. Fretigny, Analytical solutions of the heat diffusion equation for 3 omega method geometry, *J. Appl. Phys.*, **108**:086104-1–086104-3, 2010.
20. S. M. Lee and D. G. Cahill, Heat transport in thin dielectric films, *J. Appl. Phys.,* **81**:2590–2595, 1997.
21. F. P. Incropera, D. P. DeWitt, T. L. Bergman, and A. S. Lavine, *Fundamentals of Heat and Mass Transfer*, 6 ed., Wiley, Hoboken, NJ, 2007.
22. E. Pop, Energy dissipation and transport in nanoscale devices, *Nano Res.*, **3**:147–169, 2010.
23. D. G. Cahill, W. K. Ford, K. E. Goodson, G. D. Mahan, A. Majumdar, H. J. Maris, R. Merlin, and S. R. Phillpot, Nanoscale thermal transport, *J. Appl. Phys.,* **93**:793–818, 2003.
24. J. H. Orchard-Webb, A new structure for measuring the thermal conductivity of integrated circuit dielectrics, *Int. Conf. on Microelectronic Test Structures*, IEEE, Kyoto, Japan, 1991.
25. M. B. Kleiner, S. A. Kuhn, and W. Weber, Thermal conductivity measurements of thin silicon dioxide films in integrated circuits, *IEEE Trans. Electron Devices*, **43**:1602–1609, 1996.
26. K. Kurabayashi, M. Asheghi, M. Touzelbaev, and K. E. Goodson, Measurement of the thermal conductivity anisotropy in polyimide films, *J. Microelectromech. Syst.*, **8**:180–191, 1999.
27. E. T. Swartz and R. O. Pohl, Thermal resistance at interfaces, *Appl. Phys. Lett.*, **51**:2200–2202, 1987.
28. K. E. Goodson, M. I. Flik, L. T. Su, and D. A. Antoniadis, Prediction and measurement of the thermal conductivity of amorphous dielectric layers, *J. Heat Transfer*., **116**:317–324, 1994.
29. T. Borca-Tasciuc, W. L. Liu, J. L. Liu, T. F. Zeng, D. W. Song, C. D. Moore, G. Chen, K. L. Wang, M. S. Goorsky, T. Radetic, R. Gronsky, T. Koga, and M. S. Dresselhaus, Thermal conductivity of symmetrically strained Si/Ge superlattices, *Superlattices Microstruct.*, **28**:199–206, 2000.
30. J. H. Kim, A. Feldman, and D. Novotny, Application of the three omega thermal conductivity measurement method to a film on a substrate of finite thickness, *J. Appl. Phys.,* **86**:3959–3963, 1999.
31. B. Yang, W. L. Liu, J. L. Liu, K. L. Wang, and G. Chen, Measurements of anisotropic thermoelectric properties in superlattices, *Appl. Phys. Lett.*, **81**:3588–3590, 2002.
32. Z. Chen, W. Jang, W. Bao, C. N. Lau, and C. Dames, Thermal contact resistance between graphene and silicon dioxide, *Appl. Phys. Lett.*, **95**:161910–161913, 2009.
33. S. T. Huxtable, A. R. Abramson, C. L. Tien, A. Majumdar, C. LaBounty, X. Fan, G. H. Zeng, J. E. Bowers, A. Shakouri, and E. T. Croke, Thermal conductivity of Si/SiGe and SiGe/SiGe

superlattices, *Appl. Phys. Lett.*, **80**:1737–1739, 2002.

34. C. Dames and G. Chen, Thermal conductivity of nanostructured materials, *Thermoelectrics Handbook: Macro to Nano*, D. M. Rowe (Ed.), CRC Press, Boca Raton, 2005.
35. A. J. Minnich, J. A. Johnson, A. J. Schmidt, K. Esfarjani, M. S. Dresselhaus, K. A. Nelson, and G. Chen, Thermal conductivity spectroscopy technique to measure phonon mean free paths, *Phys. Rev. Lett.*, **107**:095901, 2011.
36. A. J. Minnich, Measuring phonon mean free paths using thermal conductivity spectroscopy, *Ann. Rev. Heat Transfer.,* **16**:183–210, 2013.
37. G. Chen, *Nanoscale Energy Transport and Conversion: A Parallel Treatment of Electrons, Molecules, Phonons, and Photons*, Oxford University Press, London, 2005.
38. C. Dames, Microscale conduction, *Heat Conduction*, L. M. Jiji (Ed.), Springer, New York, pp. 347–401, 2009.
39. Z. Wang, J. E. Alaniz, W. Jang, J. E. Garay, and C. Dames, Thermal conductivity of nanocrystalline silicon: Importance of grain size and frequency-dependent mean free paths, *Nano Lett*., **11**:2206–2213, 2011.
40. T. Tong and A. Majumdar, Reexamining the 3-omega technique for thin film thermal characterization, *Rev. Sci. Instrum.,* **77**:104902-1–104902-9, 2006.
41. I. K. Moon, Y. H. Jeong, and S. I. Kwun, The 3 omega technique for measuring dynamic specific heat and thermal conductivity of a liquid or solid, *Rev. Sci. Instrum.,* **67**:29–35, 1996.
42. T. Borca-Tasciuc, A. R. Kumar, and G. Chen, Data reduction in 3 omega method for thin-film thermal conductivity determination, *Rev. Sci. Instrum.,* **72**:2139–2147, 2001.
43. Y. S. Ju, K. Kurabayashi, and K. E. Goodson, Thermal characterization of anisotropic thin dielectric films using harmonic Joule heating, *Thin Solid Films*, **339**:160–164, 1999.
44. Y. S. Ju and K. E. Goodson, Process-dependent thermal transport properties of silicon-dioxide films deposited using low-pressure chemical vapor deposition, *J. Appl. Phys.,* **85**:7130–7134, 1999.
45. A. Jacquot, B. Lenoir, A. Dauscher, M. Stolzer, and J. Meusel, Numerical simulation of the 3 omega method for measuring the thermal conductivity, *J. Appl. Phys.,* **91**:4733–4738, 2002.
46. B. W. Olson, S. Graham, and K. Chen, A practical extension of the 3 omega method to multilayer structures, *Rev. Sci. Instrum.,* **76**:053901–053907, 2005.
47. S. P. Gurrum, W. P. King, Y. K. Joshi, A semianalytical solution for the 3 omega method including the effect of heater thermal conduction, *J. Appl. Phys.,* **103**:113517, 2008.
48. M. F. Ashby, *Materials Selection in Mechanical Design,* 3rd ed. (see Fig. 4.11), Butterworth-Heinemann, Oxford, UK, 2005.
49. N. W. Ashcroft and N. D. Mermin, *Solid State Physics*, Harcourt College Publishers, Orlando, Florida, 1976.
50. C. E. Raudzis, F. Schatz, and D. Wharam, Extending the 3 omega method for thin-film analysis to high frequencies, *J. Appl. Phys.,* **93**:6050–6055, 2003.
51. S. N. Schiffres and J. A. Malen, Improved 3-omega measurement of thermal conductivity in liquid, gases, and powders using a metal-coated optical fiber, *Rev. Sci. Instrum.,* **82**:064903, 2011.
52. L. Lu, W. Yi, and D. L. Zhang, 3 omega method for specific heat and thermal conductivity measurements, *Rev. Sci. Instrum.,* **72**:2996–3003, 2001.

53. P. B. Kaul, K. A. Day, and A. R. Abramson, Application of the three omega method for the thermal conductivity measurement of polyaniline, *J. Appl. Phys.,* **101**:083507, 2007.
54. E. Yusibani, P. L. Woodfield, M. Fujii, K. Shinzato, X. Zhang, and Y. Takata, Application of the three-omega method to measurement of thermal conductivity and thermal diffusivity of hydrogen gas, *Int. J. Thermophys.*, **30**:397–415, 2009.
55. S. Sangwoo, H. Tae-Jung, P. Hyung-Ho, and C. Hyung Hee, Thermal conductivity of BCC-ordered mesoporous silica films, *J. Phys. D*, **42**:125404, 2009.
56. T. Coquil, E. K. Richman, N. J. Hutchinson, S. H. Tolbert, and L. Pilon, Thermal conductivity of cubic and hexagonal mesoporous silica thin films, *J. Appl. Phys.,* **106**:034910, 2009.
57. J. Kimling, S. Martens, and K. Nielsch, Thermal conductivity measurements using 1 omega and 3 omega methods revisited for voltage-driven setups, *Rev. Sci. Instrum.,* **82**:074903, 2011.
58. N. O. Birge and S. R. Nagel, Wide-frequency specific heat spectrometer, *Rev. Sci. Instrum.,* **58**:1464–1470, 1987.
59. C. Dames, S. Chen, C. T. Harris, J. Y. Huang, Z. F. Ren, M. S. Dresselhaus, and G. Chen, A hot-wire probe for thermal measurements of nanowires and nanotubes inside a transmission electron microscope, *Rev. Sci. Instrum.,* **78**:104903, 2007.
60. C. Dames, Resistance Temperature Detectors, *Encyclopedia of Micro- and Nanofluidics*, D. Li (Ed.), Springer-Verlag, Berlin, pp. 1782–1790, 2008.
61. S. A. Putnam, D. G. Cahill, B. J. Ash, and L. S. Schadler, High-precision thermal conductivity measurements as a probe of polymer/nanoparticle interfaces, *J. Appl. Phys.,* **94**:6785–6788, 2003.
62. J. M. Ziman, *Electrons and Phonons*, Clarendon Press, Oxford, 1960.
63. G. K. White and P. J. Meeson, *Experimental Techniques in Low-Temperature Physics,* 4th ed., Oxford Science Publications, New York, 2002.
64. T. Yotsuya, M. Yoshitake, and J. Yamamoto, New type cryogenic thermometer using sputtered Zr-N films, *Appl. Phys. Lett.*, **51**:235–237, 1987.
65. D. DeVecchio, P. Taborek, and J. E. Rutledge, Matching the resistivity of Si:Nb thin film thermometers to the experimental temperature range, *Rev. Sci. Instrum.,* **66**:5367–5368, 1995.
66. R. C. Richardson and E. N. Smith (Eds.), *Experimental Techniques in Condensed Matter Physics at Low Temperatures*, Westview Press, Boulder, Colorado, 1998.
67. R. K. Chen, Personal communication, 2011.
68. J. H. Seol, I. Jo, A. L. Moore, L. Lindsay, Z. H. Aitken, M. T. Pettes, X. Li, Z. Yao, R. Huang, D. Broido, N. Mingo, R. S. Ruoff, and L. Shi, Two-dimensional phonon transport in supported graphene, *Science*, **328**:213–216, 2010.
69. A. Mavrokefalos, M. T. Pettes, F. Zhou, and L. Shi, Four-probe measurements of the in-plane thermoelectric properties of nanofilms, *Rev. Sci. Instrum.*, **78**:034901, 2007.
70. Y. C. Tai, C. H. Mastrangelo, and R. S. Muller, Thermal conductivity of heavily doped low-pressure chemical vapor deposited polycrystalline silicon films, *J. Appl. Phys.,* **63**:1442–1447, 1988.
71. D. Song and G. Chen, Thermal conductivity of periodic microporous silicon films, *Appl. Phys. Lett.*, **84**:687–689, 2004.
72. M. Asheghi, K. Kurabayashi, R. Kasnavi, and K. E. Goodson, Thermal conduction in doped single-crystal silicon films, *J. Appl. Phys.,* **91**:5079–5088, 2002.

73. F. Volklein, Thermal conductivity and diffusivity of a thin film SiO2-Si3N4 sandwich system, *Thin Solid Films*, **188**:27–33, 1990.

74. F. Volklein and E. Kessler, A method for the measurement of thermal conductivity, thermal diffusivity, and other transport coefficients of thin films, *Phys. Stat. Solidi A.*, **81**:585–596, 1984.

75. B. T. Boiko, A. T. Pugachev, and V. M. Bratsychin, Method for the determination of the thermophysical properties of evaporated thin films, *Thin Solid Films*, **17**:157–161, 1973.

76. J. E. Graebner, J. A. Mucha, L. Seibles, and G. W. Kammlott, The thermal conductivity of chemical-vapor-deposited diamond films on silicon, *J. Appl. Phys.,* **71**:3143–3146, 1992.

77. A. D. McConnell and K. Goodson, Thermal conduction in silicon micro- and nanostructures, *Ann. Rev. Heat Transfer*, **14**:129–168, 2005.

78. P. G. Sverdrup, S. Sinha, M. Asheghi, S. Uma, and K. E. Goodson, Measurement of ballistic phonon conduction near hotspots in silicon, *Appl. Phys. Lett.*, **78**:3331–3333, 2001.

79. X. Zhang, H. Xie, M. Fujii, H. Ago, K. Takahashi, T. Ikuta, H. Abe, and T. Shimizu, Thermal and electrical conductivity of a suspended platinum nanofilm, *Appl. Phys. Lett.,* **86**:171912, 2005.

80. W. L. Liu, T. Borca-Tasciuc, G. Chen, J. L. Liu, and K. L. Wang, Anisotropic thermal conductivity of Ge quantum-dot and symmetrically strained Si/Ge superlattices, *J. Nanosci. Nanotechnol.,* **1**:39–42, 2001.

81. M. Asheghi, M. N. Touzelbaev, K. E. Goodson, Y. K. Leung, and S. S. Wong, Temperature-dependent thermal conductivity of single-crystal silicon layers in SOI substrates, *ASME J. Heat Transfer*, **120**:30–36, 1998.

82. R. Venkatasubramanian, Lattice thermal conductivity reduction and phonon localizationlike behavior in superlattice structures, *Phys. Rev. B*, **61**:3091–3097, 2000.

83. W. Liu and M. Asheghi, Thermal conduction in ultrathin pure and doped single-crystal silicon layers at high temperatures, *J. Appl. Phys.,* **98**:123523, 2005.